Dynamical Climatology

Single column model tests of the Rowntree convection scheme using GATE data.

by

D. Gregory

DCTN 62

February 1988

Meteorological Office (Met. O. 20)
London Road
Bracknell
Berkshire RG12 2SZ

DYNAMICAL CLIMATOLOGY TECHNICAL NOTE NO. 62

SINGLE COLUMN MODEL TESTS OF THE ROWNTREE CONVECTION SCHEME USING GATE DATA

by

D Gregory

Met O 20 (Dynamical
Climatology Branch)
Meteorological Office
London Road
Bracknell
Berkshire RG12 2SZ U.K.

February 1988

NOTE: This paper has not been published. Permission to quote from it should be obtained from the Assistant Director of the above Meteorological Office branch.

ABSTRACT

The 11-layer single column model is used to investigate the ability of the Rowntree convection scheme to represent the effects of deep tropical convection. Comparison of the versions used in the 3rd and 4th annual cycle integrations of the 11-layer AGCM is made and the inclusion of a downdraught representation in the 4th annual cycle version investigated. The imbalance between convection and forcing processes (large-scale advection, radiation, surface fluxes) initially in the single column model integrations is investigated with respect to possible feedback processes which might occur in an AGCM.

CONTENTS

(1) Introduction

(2) The single column model

(3) The Rowntree convection scheme

(4) The TPRR(1979) data set

(5) Comparison of 3rd and 4th annual cycles

(6) Modification of the 4ac Rowntree convection scheme

(7) Summary

(8) References

(9) Notation

(1) INTRODUCTION

The aim of parametrizations is to calculate the effects of sub-grid scale processes in terms of grid-scale variables predicted by a numerical model. In general, model results are dependent upon the physical parametrizations used and much work has been undertaken in this area.

A study has been initiated of the convection scheme used at the UK Meteorological Office in the coarse and fine mesh forecast models, and the 11-layer AGCM employed in climate research. The present scheme was first described in Rowntree(1973) and recent developments are documented in Volume One of the 11-layer AGCM handbook (Slingo(1985)). Tests of the scheme in a single column model using GATE data are reported in Lyne and Rowntree(1976). However since the late 1970's little detailed study of the scheme has been carried out. The present study is undertaken with a view to possible modifications to improve the scheme's performance in the Meteorological Office atmospheric general circulation model (AGCM).

Here the ability of the Rowntree scheme to represent deep convection is investigated. Results of single column model experiments, using composite GATE data, are presented and the physical basis of the scheme investigated. The scheme's performance is compared with the observations and also with results of a recent study, using the meso-scale cloud model of Imperial College (Atmospheric Physics Group) and employing the GATE data used in the present experiments. This study of the parameterization of deep convection provides detailed information on the structure of a GATE cloud ensemble and the relative importance of the physical processes by which convection affects its large-scale environment. Observational data cannot give these details with any accuracy. (Details of the explicit cloud modelling study are to be found in Gregory(1986) and Gregory and Miller(1987), the model being first described in Miller and Pearce(1974).)

(2) THE SINGLE COLUMN MODEL

A single column version of the 11-layer model is employed in simulating the GATE atmosphere. A time step of 15 minutes is used, and the vertical grid is as specified in the 11-layer AGCM handbook (Slingo(1985), sigma co-ordinates being used. Surface pressure is specified to be 1013mb, from GATE observations, with model levels at 1000, 950, 855, 727, 585, 442, 322, 233, 160, 90, and 22mb. Initial thermodynamic and wind profiles are specified using the Thompson, Payne, Recker and Reed(1979) (TPRR(1979)) composite GATE phase III data set, described in a later section. The effects of large-scale horizontal and vertical advection (usually referred to as large-scale forcing) are specified from the observational data as cooling and moistening rates, applied to the temperature and moisture fields. The evolution of u and v are constrained to follow that observed. However in the model boundary layer (the lowest 3 layers), mixing by turbulent eddies also modifies the wind field.

The physics routines used in the single column model (SCM) are as those used in the AGCM. In these experiments they are:-

(1) Radiation-radiative fluxes are specified using the temperature and moisture profiles and cloud amounts (high, medium, low, and convective); the cloud amounts and levels are derived from the large-scale precipitation and convection schemes.

(2) Boundary layer-Clarke formulation (Clarke(1970),Carson(1982a)).

(3) Large-scale precipitation-occurs when supersaturation exists. The ice phase is considered, but no evaporation of falling precipitation (unlike the 4th annual cycle).

(4) Convection scheme-various schemes used and described in the next section.

A scheme to calculate soil temperature is also included in the SCM (including representations of soil and vegetation types), although it is unused in the experiments. The GATE area is over sea (Eastern Atlantic) and so the surface temperature is fixed at 27°C.

The boundary layer scheme calculates surface fluxes of sensible and latent heat using temperature and moisture differences between the surface and the lowest model layer. In early integrations these fluxes were found to be underestimated by 50 to 60% compared to those observed over the GATE area. To allow comparison with observations, the surface fluxes are also specified from the TPRR(1979) data set. These are added to the lowest model layer and distributed into the next two layers by the model boundary layer scheme.

(3) THE ROWNTREE CONVECTION SCHEME

This is a penetrative convection scheme, applicable to both moist and shallow convection and is at present in use in the Met. Office operational model and in the 11-layer climate model used for climate research. It was developed using GATE data (Lyne and Rowntree(1976)) and is documented in Slingo(1985). The scheme is based on parcel theory, modified by en/detrainment. The parcel represents an ensemble of buoyant plumes, each of differing characteristics. Thus parcel values of temperature, mixing ratio and mass flux are averages over the ensemble.

For a column of the atmosphere, working from the bottom upward, each layer of the model is tested until one is found which, with a slight excess buoyancy s (0.2K), is still buoyant by more than a lower limit b (set to 0.2K in the standard scheme) at the next layer after ascent, taking entrainment of environmental air into consideration. The convective process is then initiated. The initial mass flux of the parcel is proportional to the excess buoyancy,

$$M = 10^{-3}\Delta t \left\{ d + c\left[\left((\theta P_v)_{k-1} - (\theta e_v)_{k-1} \right) - b \right] / \Delta\sigma_{k-\frac{1}{2}} \right\} \qquad (3.1)$$

where θP_v is the virtual potential temperature of the parcel,

θe_v is the virtual potential temperature of the environment,

Δt is the centred timestep of the model,

$\Delta\sigma_{k-\frac{1}{2}} = \sigma_k - \sigma_{k-1}$

and d and c are empirical constants set to 0.0 and $3.33\times10^{-4}s^{-1}$ in the standard scheme.

(Note that k decreases with height.)

Ascent continues upward, the parcel entraining environmental air at levels k-¼, k-¾ at a fractional entrainment rate of

$$\varepsilon_{k-1/4}=3A_E\sigma_k(\sigma_k-\sigma_{k-1/2})$$

$$\varepsilon_{k-3/4}=3A_E\sigma_{k-1/2}(\sigma_{k-1/2}-\sigma_{k-1}) \qquad (3.2)$$

where $A_E=1$ if $k=11$ (lowest layer)

and $A_E=1.5$ if $k<11$

In the 4th annual cycle scheme mixing detrainment of cloud air into the cloud environment is considered to occur in layer k at a rate of,

$$\eta_k=(\varepsilon_{k-1/4}+\varepsilon_{k-3/4})(1-A_E^{-1}) \qquad (3.3)$$

If on ascending from layer k to k-1 the excess buoyancy of a parcel is found to be less than the lower limit set by the empirical parameter b, forced detrainment occurs at a rate δ_k. It is assumed that a proportion of the less buoyant members of the ensemble terminally detrain in layer k, increasing the excess buoyancy of the parcel in layer k-1 to b (virtual temperature being used throughout). Assuming that the detraining clouds do so at zero buoyancy, with the above assumptions the potential temperature of the detraining air, θ^r, may be calculated using the Clausius-Clapeyron relation, together with the rate at which detrainment occurs and θp_{k-1}. (See Slingo(1985) for details.)

The process of forced detrainment allows buoyancy to increase indefinitely and so it is necessary to limit it by two considerations which terminate the convective process. Firstly, a parcel is not allowed to ascend higher than an undilute parcel from the starting level. Secondly, it is reasonable to assume that if the convective mass flux fall below a minimum value defined by,

$$M_{min}=10^{-3}cE_{min}\Delta t \qquad (3.4)$$

where E_{min} is 1K in the standard scheme,

then the parcel is destroyed by entrainment.

The process of terminal detrainment from the plume is handled differently in the 3rd annual cycle from the 4th. In the 3ac, the parcel is assumed to detrain totally at level k with parcel values θ^p_k, q^p_k. In the 4ac the parcel detrains at level k with neutral buoyancy, the remainder detraining at level k-1 with parcel values.

The plume interacts with its environment through en/detrainment and subsidence which compensates for the parcel's upward mass flux. Considering fluxes of θ and q between cloud and environment in layer k and vertically out of and into layer k, the net change in a time Δt of the environmental potential temperature, θ^e_k, and specific humidity, q^e_k, are given by,

$$\Delta\theta^e_k=((M_k/\Delta t)\Delta t/\Delta\sigma_k)\{(1+\varepsilon_k-\tfrac{1}{4})(1-\delta_k)(1-\eta_k)(\theta^e_{k-1}-\theta^e_k) \tag{3.5}$$
$$+\delta_k(1-\eta_k)(\theta^r_k-\theta^e_k)+\eta_k(\theta^p_k-\theta^e_k)\}$$

$$\Delta q^e_k=((M_k/\Delta t)\Delta t/\Delta\sigma_k)\{(1+\varepsilon_k-\tfrac{1}{4})(1-\delta_k)(1-\eta_k)(q^e_{k-1}-q^e_k) \tag{3.6}$$
$$+\delta_k(1-\eta_k)(q^r_k-q^e_k)+\eta_k(q^p_k-q^e_k)\}$$

The first term in these expressions represents compensating subsidence, the second and third forced and mixing detrainment respectively, the latter being only present in the 4ac scheme ($\eta_k=0$ in the 3ac version).

These expressions for $\Delta\theta^e_k$, Δq^e_k do not take into account the evaporation of precipitation and detrained liquid water nor the melting/freezing of falling precipitation. Two differing schemes are employed in the 3ac and 4ac to model condensation, evaporation and precipitation.

(a)3ac In this version any condensate is assumed to fall out immediately as snow if the temperature of the layer is below -10°C, otherwise as rain. The condensation (in cm) produced in taking the ensemble from level k to k-1 is given by,

$$P_k=(q^{P}_{k-1}-q_s(\theta^{P}_{k-1}))M_{k-1}[10p_*/g] \qquad (3.7)$$

if the parcel is saturated at level k-1.

The parcel mixing ratio is adjusted after condensation such that $q^{P}_{k-1}=q_s(\theta^{P}_{k-1})$.

In order to allow for cloud dissipation and the effects of unsaturated downdraughts on falling precipitation, some evaporation takes place in level k,

$$E_k=e[q_s(\theta^{e}_{k})-q^{e}_{k}]M_{k-1}[10p_*\Delta\sigma/g] \qquad (3.8)$$

where e is a constant (referred to as evcon later).

The environmental humidity and temperature are then incremented by

$$\Delta q^{e}_{k}=gE_k/(10p_*\Delta\sigma_k)$$

$$=e[q_s(\theta^{e}_{k})-q^{e}_{k}]M_{k-1} \qquad (3.9)$$

$$\Delta T^{e}_{k}=-(L/c_p)\Delta q^{e}_{k}$$

Further temperature increments occur as the precipitation crosses the freezing level. The evaporation process is limited by the constraint,

$$E_k \leqslant P_k$$

The total precipitation at the ground is obtained by summing eqn(3.7) and eqn(3.8) over all levels.

(b)4ac Precipitation of condensed water does not occur until the cloud has exceeded a critical depth, D_{crit} (base to top) and the amount of cloud condensate within the parcel (X^P_k) exceeds a minimum value X_{min}. If these criteria are not met, water is stored within the parcel and the ascent continues (if possible). This allows the possibility of cloud liquid water being detrained into the environment causing increments to the moisture and temperature field of

$$\Delta q^e_k = (\delta_k + \eta_k(1-\delta_k)) M_k X^P_k / \Delta\sigma_k$$

$$\Delta T^e_k = -(L/c_p)\Delta q^e_k \qquad (3.10)$$

In the standard scheme X_{min} is set to 1g/kg or the local saturation specific humidity where it is less, while D_{crit} is defined by,

$$D_{crit} = \begin{cases} 4.0\text{km over land} \\ 1.5\text{km over sea} \\ 1.0\text{km if } T_{k-1} < 263\text{K} \end{cases}$$

If these criteria are met the amount of precipitation produced in cm in taking the ensemble from level k to k-1 is,

$$P_k = (X^P_{k-1} - X_{min}) M_{k-1} (10 p_*/g) \qquad (3.11)$$

X_{min} of the condensate is retained by the parcel in the process.

Total precipitation falling from cloud base is given by,

$$J_b = \sum_{k=\text{cloud base}}^{k=\text{cloud top}} P_k \qquad (3.12)$$

Falling snow is not evaporated. Evaporation of falling rain occurs only below cloud base, the rate being proportional to $(q^e_k - q_s(\theta^e_k))$ and is constructed by integrating the fractional evaporation of precipitation over a layer of depth dz ie,

$$dJ/J=\beta(q-q_s)\rho dz/Q \qquad (3.13)$$

where ρ is the density of air, Q is the local rainfall rate estimated by assuming precipitation covers 10% of a grid box and β is a constant set to $10^{-3}s^{-1}$ in the standard scheme.

If the air is not saturated the precipitated water J_k reaching level k from level k-1 is given by,

$$J_k=J_{k-1}\exp[-10\Delta t p_* \Delta\sigma_k[q_s(T^c_k)-q^e_k]/[J_b g]] \qquad (3.14)$$

Once all the increments have been calculated a check is made to ensure enthalpy is conserved,

$$c_p\int_1^0 \Delta T d\sigma + L\int_1^0 \Delta q d\sigma = L_F\int_1^0 \Delta_s q_f d\sigma \qquad (3.15)$$

where L_F is the latent heat of fusion,

q_f is the ice content,

and Δ_s is the increment due to changes in phase only.

This integral is satisfied by reducing the temperature increments of the same sign as the residual.

(4) THE TPRR(1979) DATA SET.

Few good complete observational data sets exist of deep convection. One commonly used is that of Thompson, Payne, Recker and Reed(1979) (TPRR(1979)). This is a composite analysis of easterly waves occurring during phase III (August to September 1974) of the GATE experiment.

Easterly waves are weak disturbances in the ITCZ travelling from east to west. They occur in the summer months over the Atlantic, West Africa and western Pacific and form by joint baroclinic-baratropic instability on the mid-tropospheric easterly jet. Much of the cloudiness of the ITCZ in these regions is attributable to these features and convection is thought to play an important role in their maintenance over the Pacific. Atlantic easterly waves have a wave length of 2500km and propagate to the west at $8ms^{-1}$. A clear wave structure is observed in the meridional flow. Northerlies occur ahead of the surface trough sloping westward with height. Ahead of the ridge the converse structure is seen. Convection is most active near the wave trough associated with maximum upward motion on the synoptic scale. Subsidence and a drier atmosphere causes convection to be suppressed in the ridge. (TPRR(1979) discuss structural differences between Altantic and Pacific easterly waves. These are due in part to differences in the basic flow over the two areas.)

TPRR present a composite wave of approximately 80 hours duration. Eight wave categories are defined, category 8 being when the ridge of the wave is over the GATE area, category 4 the trough. The SCM thermodynamic profiles are initialised with data from 2.5 hours into the data set (during category 1 and referred to as 0 hours of the simulation). A T-φgram of temperature and mixing ratio profiles is presented in fig 1 (with u and v profiles) interpolated to model levels. If air is lifted from the lowest model level ($\approx$1000mb) saturation occurs at 955mb with free convection at $\approx$950mb. A deep layer of instability exists. With undilute ascent from the surface zero buoyancy occurs at 150mb, showing deep convection is possible once initiated.

Vertically and horizontally integrated budgets of cooling and moistening due to large-scale horizontal and vertical advection are shown in table 1. Profiles of these quantities are presented to the model every 10 hours (through a wave cycle of 80 hours), with linear interpolation between. The 10 hour averaging periods are displaced by 2.5 hours from those of TPRR. However the 70-80 hour average contains the ridge of the wave, 30-40 hours the trough. Surface fluxes are also shown, latent heating being dominant over sensible heating, together with the observed surface rainfall.

Figure 2 shows the evolution of total moisture convergence and surface evaporation compared to surface rainfall with time. Rainfall is a minimum in the ridge and maximum just after the passage of the trough. Surface rainfall does not follow the moisture forcing, large amounts of moisture being stored in the atmosphere during the first half of the wave and being rained out in the second half. Such a feature is common to easterly waves and is poorly modelled by parameterization schemes.

Vertical profiles of large-scale forcing are shown in fig 3. Large-scale cooling peaks around 600mb, with a maximum moistening in the lower atmosphere (≃900mb). Also shown are the apparent heat source (Q1) and moisture sink (Q2) due to diabatic processes (excluding radiation) calculated from the advective fluxes. These are defined as;

$$\pi Q1 \simeq \pi\left\{\frac{L\bar{Q}}{c_p\pi} - \frac{\partial\overline{\omega'\theta'}}{\partial p}\right\}_{CONV} - \pi\left\{\frac{\partial\overline{\omega'\theta'}}{\partial p}\right\}_{BL} + \pi\left\{\frac{L\bar{Q}}{c_p\pi} - \frac{\partial\overline{\omega'\theta'}}{\partial p}\right\}_{LSR}$$

$$Q2 = \left\{-\bar{Q} - \frac{\partial\overline{\omega'q'}}{\partial p}\right\}_{CONV} - \left\{\frac{\partial\overline{\omega'q'}}{\partial p}\right\}_{BL} + \left\{-\bar{Q} - \frac{\partial\overline{\omega'q'}}{\partial p}\right\}_{LSR} \qquad (4.1)$$

where φ is a large-scale area average of φ (or grid point value),

$\varphi' = \varphi - \bar{\varphi}$,

Q is the net condensation/evaporation rate,

π is $(p/p_*)^{R/c_p}$ where p_* is a reference pressure (taken to be p_{**} in the SCM),

CONV refers to convective processes,

BL refers to surface fluxes and boundary layer processes, and LSR refers to large-scale moist processes.

(Similar quantities can be defined in sigma co-ordinates.)

The vertical structure of Q1 and Q2 generally follow those of the large-scale forcing. Surface rainfall, profiles of Q1 and Q2 and the observed vertical structure of the atmosphere will be compared to results obtained from the SCM.

(5) COMPARISON OF 3RD AND 4TH ANNUAL CYCLE.

Several experiments using the SCM were performed to compare the performance of the 3rd and 4th annual cycle versions of the Rowntree convection scheme using the GATE data described in section(4).

Several 20 day integrations of the SCM were performed covering 6 cycles of the GATE data (6 wave cycles). Constants within the convection scheme were changed between integrations to test the sensitivity of the schemes. Table 2 lists the experiments performed and the constants varied (all other constants have their standard values-see Slingo(1986)).

Figure 4 presents 10 hour averages of surface rainfall (convective plus large-scale) for these experiments composited over wave cycles 2 to 6 (80 to 480 hours model time). Wave cycle 1 is also shown, but is not included in the averages as initially more rain is produced than in the equivalent period of the later wave cycles (fig 4a) due to the large convective instability which exists in the initial profile. This causes an earlier peak in the rainfall resulting in over stabilization and an early reduction in rainfall. However towards the end of the first wave cycle rainfall values are similar to those observed later in the simulation.

Experiments X1 and X2, involving the 3ac, follow the specified forcing closely (fig 4b). Contrary to observations little moisture storage occurs in the first half of the wave cycle. Hence the peak surface rainfall occurs approximately 10 hours before the time observed.

Experiments X3 and X4 (utilizing the 4ac) do not follow the applied forcing as closely as experiments with the 3ac scheme. Minimum and maximum rainfall occur up to 10 hours later in the 4ac, indicating greater storage of moisture. For both the 3ac and 4ac convection schemes the change in constants produces little change in the evolution of the rainfall.

Both schemes reach a balance with the applied moisture forcing (table 3) when averaged over the entire composite wave, raining out

approximately 360Wm^{-2} (12.4mm/day) compared to a net moisture input of 370Wm^{-2} (12.8mm/day).

The ability of both schemes to reach equilibrium is due to modification of the model thermodynamic profile during the first few hours of the simulation. Initially the convective latent heat release is greater than the cooling and moistening of the applied forcing. This is clearly seen in the evolution of temperature and mixing ratio in the lowest model layer (centred at 1000mb) (fig 5, 10 hour averages plotted). The model profiles proceed to a 'preferred' quasi-steady state where a balance between convection and applied forcing is possible. A quasi-cyclic behaviour over each wave cycle is seen although it is not of the same nature as observed; maximum moistening occurs when rainfall is maximum (generally) whereas the observations (also plotted in fig 5) suggest the contrary. For each scheme the new steady state is different due to the differing physics represented in both.

There are changes not only in the lowest model layer but also in the entire thermodynamic profiles. Table 4 shows temperature and moisture profiles (for integration X2 and X3) averaged over the first wave cycle and over wave cycles 2 to 6, compared to the observed wave cycle mean. Throughout the cloud layer (cloud top being mainly level 4 but occasionally level 3-levels are defined in table 4) the two averages (for T and q) have similar structures. Thus the preferred structure is reached early in the integration. Large differences exist above the cloud layer due to radiative and applied forcing being unbalanced by any other physical process.

The evolution of the thermodynamic profiles is also cyclic in character within the cloud layer. Figure 6 shows the evolution of T and q composited over wave cycle 2 to 6 together with the observed evolution, for integrations X2 and X3. Deviations tend towards zero at the end of the wave cycle. Different evolutions are seen throughout the wave cycle, attributed to the differing physics in the two versions of the convection scheme.

Considering experiments X1 and X2 involving the 3ac scheme, comments have already been made regarding the simulated distribution of rainfall through the wave (fig 4). For experiment X2 the atmospheric temperature structure is reasonably represented (table 4 and fig 6) although a large drying is seen at the surface (fig 5) and in the next few layers above. This drying occurs rapidly after the start of the simulation and is caused, in the lowest layer, by too little evaporative moistening from precipitation which, together with the effects of surface fluxes is insufficient to balance subsidence drying. Such a drying would soon inhibit convection but this is compensated by the lowest two layers becoming unstable with respect to dry ascent. Thus convection occurs although the saturation level is higher than observed (≃930mb cf 960mb). This results in a lower saturated equivalent potential temperature (θ_{ES}) on moist ascent. Cooling below 700mb compensates for this somewhat allowing the parcel to remain buoyant as it ascends. Initially convective heating peaks too high in the atmosphere (≃500-400mb) compared to the forcing (≃600mb). This leads to warming of the upper troposphere increasing forced detrainment and causing the mass flux to peak around 700mb. This gives a maximum Q1 at ≃600mb, with Q2 peaking nearer the surface (≃900mb) due to the increase in $|\partial q/\partial p|$ towards the surface (fig 7). This change bring the profiles of Q1 and Q2 into better agreement with the observations (fig 3).

Table 5 compares temperature and moisture profiles averaged over wave cycles 2 to 6 for experiments X1 and X2. Both experiments have similar structures in the vertical although differences are noted. With evcon=3 a warmer, drier atmosphere exists in the steady state compared to X2 where evcon=9. The difference is predominantly caused by less evaporation of rain initially. Both experiments underestimate the static stability ($\partial\theta/\partial p$) of the boundary layer. The observed static stability between 1000mb and 850mb is 3.31×10^{-2}K/mb; X1 and X2 underestimate this by 20 and 10% respectively. Greater errors are seen between the two lowest levels (1000 and 950mb). Here $\partial\theta/\partial p$ is observed to be 8×10^{-3}K/mb while X1 and X2 show $6\times10^{-3}$and 4×10^{-3}K/mb respectively. However compared to the 4th annual cycle integrations (shown later) the 3rd annual cycle convection scheme retained the temperature structure of the boundary layer well.

From the explicit cloud model study described in the introduction, contributions of updraught, downdraught and detrainment of cloud condensate to both budgets and profiles of Q1 and Q2 can be determined with some certainty (Gregory and Miller(1987)). (Only periods 0 to 10 and 20 to 30 hours were simulated in this study.) Table 6 compares the sensible heat budget of the 3ac experiment for wave category 3 (20-30 hours) composited for wave cycles 2 to 6 with the results from the explicit model. Definitions of the terms compared are given in the table. Explicit model results show that updraughts warm the atmosphere twice as much as the net value of Q1, downdraughts and detrainment evaporation balancing the excess. Using evcon=9 the results agree well with explicit model.

For wave category 1 (0-10 hours) the 3ac scheme gives values of UD/Q1 and (DD+DEVP)/Q1 of 2.6 and -1.6 respectively (using evcon=9), similar to those for wave category 3. However these are in disagreement with the explicit model which gives values of 3.3 and -2.3 for the same period. The difference arises from the observation that during wave category 1 much of the moisture supplied by the large-scale and surface forcing is stored within the atmosphere and convection inhibited. The explicit model represents this well suggesting the effect to be caused by the dissipation of growing convective towers ascending through the relatively dry atmosphere of the ridge. The Rowntree scheme only represents entrainment and detrainment from fully grown convective towers and not entrainment during the growing stage. Hence the SCM results do not represent this well in the 1 to 10 hour average.

Figure 7 shows the evolution of Q1 and Q2 averaged over wave cycles 2 to 6 (for integration X2). Again the applied forcing is nearly balanced at all levels, Q1 and Q2 agreeing reasonably well with those observed during GATE (fig 3). (Q1 exceeds the large-scale forcing throughout much of the wave the deficit being made up by radiation which over the 20 days of the integration contributes a net cooling of $\simeq -80 Wm^{-2}$ in both experiments.) Figure 8 shows the contributions of various terms to the vertical distributions of Q1 and Q2 for the same experiment (for the period 20-30 hours composited over wave cycles 2 to 6). Also plotted are contributions to Q1 from UD, DD and DEVP calculated from the explicit cloud model. (The

Q2 budget is not compared as not all the terms in the scheme and explicit model budgets are directly analogous.) For Q1 the profiles agree well, subsidence heating having a similar shape and magnitude to that seen in the explicit model updraught. The EVP term of the 3ac scheme compares well with contribution of DD and DEVP of the explicit model, indicating that this term produces a reasonable representation of a convective downdraught (for more discussion of this see section 6). (It must be noted that the lower boundary of the explicit model is at 1000mb and saturation is seen at the lowest model level (975mb) under convective cloud, giving a poor representation of cloud base. This is associated with the vertical resolution of the model (50mb) which is not adequate enough to simulate the sub-cloud layer well. Hence the explicit model can say little concerning the physics of the lowest layer of the SCM (1000mb).)

Turning to the 4ac integrations (X3 and X4) a different steady state structure is reached to that of the 3ac experiments (table 4). Magnitudes of the deviations are however similar. Warming is seen to occur in the mid- to upper troposphere causing increased forced detrainment and bringing the Q1 and Q2 profiles into agreement with the observations as previously discussed. The evaporation of falling precipitation, now only below cloud base (in this instance the lowest model layer) causes considerable moistening and cooling. Again the preferred structure repeats every 80 hours as seen in the time evolution of T and q for the 1000mb layer (fig 6).

The cooling of the lowest model layer causes the boundary layer to be come excessively stable with respect to dry ascent, inhibiting the initiation of convection. Although saturation occurs in the second model layer (lifting from the lowest model layer) the parcel is buoyant only through virtual effects. This causes the different time evolution in rainfall (fig 4) through the wave cycle compared to the 3ac integration already noted. The stabilization of the two lowest model layers causes convection to be inhibited in the first half of the wave cycle, delaying the warming of the model atmosphere by 10 to 20 hours (fig 6). This causes greater moisture storage during the first half of the wave cycle than in the 3ac integrations.

Although such moisture storage and delay in rainfall compared to the growth of large-scale moisture forcing in the early part of the wave is observed, the mechanism by which it is achieved in the SCM experiments is unrealistic. As discussed previously storage is achieved in reality by the weakening of growing convective towers through the entrainment of the relatively drier air of the ridge, rather than through the evaporation of rain and the stabilization of the boundary layer.

The effect of decreasing the constant c used to determine the initial mass flux ten fold (integration X4) has little effect upon the rainfall distribution (fig 4c). The lowest model layer is slightly warmer and moister, T and q (previously defined in table 4) being 297.6K and 18.6g/kg respectively. This compensates somewhat for the reduction in the value of c allowing saturation to occur lower in the atmosphere. Above this little difference was found in the thermodynamic profiles.

When integrated over wave cycles 2 to 6 the surface rainfall for experiments X3 and X4 was little different (table 3). Comparison of the contributions to the Q1 budget of the 4ac convection scheme and those diagnosed from the explicit cloud model is made in table 7 for 20-30 hours. (Note the change in definition when referring to UD, DD and DEVP for the 4ac scheme from those in table 6 for the 3ac scheme. Definitions for the explicit cloud model are identical in both tables.) Similar ratios are observed for other parts of the wave although a slight increase in the evaporation of precipitation occurs in the ridge of the wave. Evaporation of detrained cloud condensate exceeds that of falling precipitation indicating that the new evaporation scheme gives a poor representation of deep convective downdraught processes.

The evolution of the vertical profiles of Q1 and Q2 for experiment X3 is presented in fig 9 and similar to the results for experiment X2, Q1 and Q2 approximately balancing the forcing. Figure 10 shows the contributions that various physical processes make to the profiles of Q1 and Q2 for 20-30 hours. Comparison with explicit model results (fig 8) is not good. Because there is little evaporation in the lower troposphere CS has to peak around 600mb to balance the forcing. Detrainment of cloud condensate

occurs at mid- and high-levels, agreeing with the results of observations and of the explicit cloud model study which indicate two major outflow layers in the mid- and high-troposphere (not shown). This detrainment causes saturation of the model at high levels and an increase in large-scale rain between the 3ac and the 4ac SCM integrations (table 8). Large stratiform anvil clouds are known to form in the tropics associated with convection and give considerable rainfall. Cheng and Houze(1979) estimate that ≃40% of GATE rainfall was from such features. Such features are dynamically active with gradual ascent and are thick (≃500mb-150mb). Hence the relatively thin stratiform cloud within the SCM cannot be considered to represent these features.

After considering both the 3ac and the 4ac versions of the Rowntree scheme which is to be preferred? Both balance the applied forcing giving similar amounts of rainfall integrated over the wave. A reasonable atmospheric structure is retained by both schemes. The 4ac version keeps the lowest model layer moist but produces a very stable boundary layer. The 3ac version reproduces the boundary layer temperature reasonably well in the vertical but produces excessive drying of the boundary layer. Both versions warm the upper troposphere producing a more stable atmosphere to moist ascent.

These structures are obtained with specific forcing (apart from radiation) and feedbacks in an AGCM may compensate for more drastic changes. However in experiments where the surface fluxes were determined by the model, a continuous drift towards a cooler, drier atmosphere was seen. This is caused by the failure of the boundary layer scheme to reproduce the magnitude of the observed surface fluxes and so balance the convective drying of the lowest model layer, causing a drift towards lower θ_E values on saturation and therefore a general cooling allowing deep convection to continue balancing the large-scale forcing. This drift may not be important in an AGCM. The low surface fluxes may be caused by an incorrect specification of the low level wind which was extrapolated from observational data at higher levels. Study of surface fluxes from integration of the 11-layer AGCM indicates that surface fluxes over oceans are generally well represented. Also in the single column model the large-

scale forcing is fixed allowing no feedback as convective activity decays. Such feedbacks may cause large-scale forcing to decay as convection reduces and so a drift towards a cooler atmosphere would not occur.

Considering the detailed physical processes represented by each scheme the 3ac version with evcon=9 is preferred (at least for tropical deep convection), the evaporation scheme representing downdraught processes reasonably well.

(6) MODIFICATION OF THE 4AC ROWNTREE CONVECTION SCHEME.

In this section modifications in an attempt to improve the physical basis of the 4ac version of the Rowntree convection scheme are discussed. Two main areas are considered;

(a) Inclusion of a downdraught representation into the 4ac version,

(b) The spin-up problem.

(a) Inclusion of a downdraught representation into the 4ac version.

Results from section(5) showed that the 4ac scheme contained a poor representation of convective downdraughts. The 3ac version of the scheme which contained a simple representation of the evaporation of falling precipitation gave better results. It would therefore seem reasonable to consider incorporating a scheme similar to the 3ac evaporation scheme into the 4ac version.

Explicit model results show that evaporation of falling precipitation is dominant in downdraughts over mechanical transports of heat and moisture. Hence it should be possible to consider only the process of evaporation in a simple downdraught model and not have to calculate a mass flux profile for the feature.

The method used in the 3ac version cannot be directly incorporated into the 4ac version. In this, precipitation is inhibited until cloud depth exceeds a critical depth, ranging from 4km over land to 1.5km over sea (or when the parcel temperature falls below 263K). Thus if evaporation only occurs in the layer below which precipitation formed (as in the 3ac version), no evaporation might occur over several layers near the surface perhaps with consequences for the lower level moisture field seen in the 3ac integrations.

A more realistic approach would be to consider the evaporation of precipitation as it falls to the surface. The 3ac evaporation method is used as a starting point. In this evaporation is given by,

$$E_k = e[q_s(\theta^e{}_k) - q^e{}_k]M_{k-1}[10p_*\Delta\sigma_k/g] \quad [cm] \quad (6.1)$$

where e is a constant (referred to as evcon.)

Subsituting for M_{k-1} from eqn(3.7) after rearrangement,

$$E_k = e\Delta\sigma_k\{[q_s(\theta^e{}_k) - q^e{}_k]/[qP_{k-1} - q_s(\theta P_{k-1})]\}P_k \quad [cm] \quad (6.2)$$

Thus evaporation in layer k is proportional to the precipitation, P_k, produced as the parcel ascends from layer k to k-1, the proportionality factor being determined by the sub-saturation of the environment in layer k compared to the amount of liquid water condensed out in the ascent from k to k-1 and the empirical constant e (evcon). This is similar in some respects to the formulation of rain water evaporation in the Kessler microphysics scheme,

$$E = \beta(q_s - q) \quad (6.3)$$

where β is a constant whose value varies with precipitation rate.

Considering now the evaporation of precipitation as it falls to the surface, by analogy to the 3ac evaporation scheme,

$$E_k = e\Delta q_k\{[q_s(\theta^e{}_k) - q^e{}_k]/(WT)_k\}(PT)_k \quad [cm] \quad (6.4)$$

where $$(PT)_k = \sum_{j=k_T}^{j=k-1}(P_j - E_j) \quad (6.5)$$

$$(WT)_k = \sum_{j=k_T}^{j=k-1}\{(P_j/e\Delta\sigma_j M_j) - (E_j/(PT)_j)(WT)_j\} \quad (6.6)$$

and k_T = level of cloud top.

(Note that $k_T < k$ and that k decreases with height)

The new evaporation scheme has been tested in the SCM using GATE data. Setting evcon=9 produced the best agreement with explicit cloud model results and these are presented.

The evolution of rainfall through the wave cycle (fig 11) follows the moisture forcing closely with small amounts of storage occurring in the first half of the wave cycle. The lowest layer reaches a new steady state (fig 12) showing cooling and slight drying. The magnitude of the cooling averaged over wave cycles 2 to 6 is greater than both 3ac and 4ac experiments. However the moisture content at 1000mb is better retained than in either of these cases (see table on fig 12). The temperature structure (table 9) is similar to that of the 3ac integrations but the moisture structure is better retained than in the previous integrations. Saturation occurs at 965mb with free convection around 950mb. These values compare well with the observed values (table 10). The evolution of temperature and moisture structure over the wave cycle is shown in fig 13. The pattern is broadly similar to that of the 3ac convection scheme results (fig 6(b)) although the amplitude is larger.

Use of evcon=3 in the evaporation formula results in a warmer and significantly drier lowest model layer after 20 days (298.9K and 15.1g/Kg compared to 296.9K and 16.4g/kg for evcon=9) caused by less evaporation. Above the boundary layer little difference is seen.

The vertical distributions of Q1 and Q2 are similar to the 3ac experiments and agree reasonably with those observed, Q1 peaking around 600mb and Q2 800mb when convection is active (fig 14). Comparison of the contributions of various physical processes represented in the modified scheme to results of the explicit cloud model is made in table 11 and fig 15 for 20-30 hours of the wave cycle. Agreement of the budgets is good being similar to the 3ac experiment budgets. However the contribution of physical processes to the vertical structure is a mixture of that seen in the earlier 3ac and 4ac experiments. The downdraught effect is similar to that of the 3ac precipitation evaporation scheme (fig 8) but evaporation in

the lowest model layer agrees with the 4ac scheme (fig 10), thus retaining the moist state. Magnitudes of subsidence and evaporation are in better agreement with the explicit cloud model than previous integrations. Detrainment of cloud condensate is different to the explicit model results, being similar to the 4ac experiments and peaking in layers where large amounts of forced detrainment occurs. In these layers evaporation into downdraughts is reduced to zero as they are saturated or near saturated.

The amount of large-scale rain is also similar to the 4ac SCM results ($8 Wm^{-2}$ compared to $299 Wm^{-2}$ for convective rain-compare with table 8). This is caused by the saturation of the upper model layers by forced detrainment of cloud condensate early in the simulation.

The inclusion of a simple downdraught representation into the present 4ac convection scheme based on the evaporation of falling precipitation brings improvement to the physical basis of the scheme. Results are generally similar to the 3ac scheme indicating that the evaporation scheme in this, on which the new one is based, was a reasonable representation of a deep convective downdraught. However an improved moisture structure results from the greater evaporation below cloud base with the new method. The vertical distribution of updraught and downdraught heating is in good agreement with the results of the explicit cloud modelling study described in the introduction.

(b) <u>The spin-up problem.</u>

The results presented in previous sections show that a modification of the model thermodynamic profile occurs within the first 10 to 20 hours of the simulation. With the variants of the Rowntree convection scheme presented, this generally results in a warming of the mid-troposphere causing more forced detrainment and so a reduction in mass flux in the upper troposphere, allowing convection to balance the applied forcing.

Such a rapid modification could have adverse consequences if it occurs within an AGCM or forecast model. A net warming of the model atmosphere

could cause an unstable feedback with increased grid scale convergence and ascent, which may lead to increased convective rainfall. Hence it is desirable that the impact of the convection scheme upon the model atmosphere should be initially small.

Figure 16 compares the initial evolution of the SCM temperature profile for the 4th annual cycle scheme and that containing the downdraught representation (described in the previous section) together with the observed evolution over the first 40 hours of the wave. The integrated temperature in the cloud layer (layer 11 to 4) is also shown. The standard 4th annual cycle scheme is seen to warm much of the atmosphere in the first 20 hours generally giving a net warming early in the simulation. With the magnitude of the large-scale ascent increasing in the first part of the wave this may lead to the feedback described above. With the modified scheme the atmosphere is cooled the structure being similar to that observed, although the deviations are larger. Cooling of the model atmosphere could perhaps lead to the reverse feedback although with increasing large-scale ascent (as in this instance) this is probably the more stable situation.

The modification of the initial profile is caused by an imbalance between the convection scheme and the applied forcing. Concentrating upon the modified 4th annual cycle scheme (hereafter denoted by 4ACM) the warming in the mid- and upper-troposphere is caused by the initial convective massflux profile peaking in these regions rather than the lower troposphere, as for the GATE area. This produces more precipitation than observed and hence too much evaporative cooling in the lower troposphere.

Several attempts have been made to rectify these problems although at the time of writing results have been disappointing. Some of the techniques investigated are discussed below.

As commented earlier the warming in the mid- and upper-troposphere during the early stages of the simulation reduces parcel buoyancy causing greater forced detrainment and brings Q1 and Q2 into agreement with the observations. Hence methods by which parcel buoyancy maybe initially

reduced in these regions, bringing the massflux maximum down into the lower troposphere, are desirable. Thus the inclusion of water loading into the calculation of parcel buoyancy was considered.

The water retained by the parcel was increased to 3g/Kg after consideration of explicit cloud model results. However buoyancy was not reduced sufficiently in the mid-levels to give the increased detrainment required. The change also caused the evaporation of detrained liquid water to be excessively large.

On reflection a realistic description of water loading is probably beyond the scope of the simple cloud microphysics employed in the Rowntree scheme. The water content of detrained cloud air is probably less than that of an active cloud parcel and so the detrainment processes are also unrealistic.

A similar solution would be to adjust the en/detrainment rates to give a more realistic mass flux profile. This could be achieved by specifying the en/detrainment structure to achieve the desired effect.

Several experiments were carried out with a modified en/detrainment structure based upon explicit cloud model results. These show an inflow region in the lowest 200mb of the atmosphere with a detrainment region above linked to terminal detrainment from different height clouds (represented in the Rowntree scheme by forced detrainment). To represent this structure mixing detrainment is reduced in the lowest 3 layers of the model and made to exceed mixing entrainment above this. The explicit cloud model indicates that for deep convective cloud a flat mass flux profile exists in the mid-levels of the troposphere indicating little net en/detrainment occurs. The modified rates above the lowest 3 layers of the model reflect this (table 12).

Figure 17 shows the initial evolution of model temperature for several of these experiments. Some readjustment of the massflux parameter (c) and evaporation constant (e) was carried out throughout the series. Generally results are disappointing. Using the en/detrainment structure of

experiment (b) gives an updraught heating profile in reasonable agreement with the explicit model initially, but fails to give significant improvements in the temperature evolution.

Improvement in the lower troposphere is obtained when the problem of over active downdraughts is considered. Using evcon=9 gives an initial ratio of updraught to downdraught heating (UD/DD) of 1.8 increasing to 2.4 later in the simulation in agreement with the explicit model results (averaged over wave cycles 2 to 6 - table 11). The increase is due to a failure to retain the initial humidity structure of the atmosphere. Moistening occurs to around 90% relative humidity throughout much of the cloud layer from an initial state where values of 70 to 50% are seen in the mid- and upper-troposphere.

Using a lower value for evcon gives better results initially (evcon=6 gives UD/DD of 2.4 initially). However moistening still occurs and UD/DD suffers. Using a variable evcon (decreasing upwards) retains a better relative humidity structure with improved cooling in the lower troposphere (fig 17(c)).

The results presented illustrate the difficulty of tuning the convection scheme to balance the large-scale and radiative forcing initially. Further work is required if a satisfactory solution is to be obtained.

(7) SUMMARY.

The ability of various versions of the Rowntree convection scheme to simulate the effects of tropical deep convection has been investigated. Using a composite easterly wave data set from GATE the performance of the scheme has been compared with observations. Diagnosis of the mechanisms by which the convection scheme interacts with the large-scale atmosphere was carried out and the results compared with a similar analysis using an explicit cloud model. This technique proved useful in identifying areas where the scheme could be improved. Modifications to the 4ac scheme improving its physical basis and performance in the 11-layer SCM have been discussed. Work is in progress to test the impact of these changes upon the climatology of the 11-layer AGCM.

(8) REFERENCES.

Carson, D.J. 1982a — Comments on the sensitivity of numerical simulations to different parameterizations of the boundary layer properties and processes. Workshop on Planetary Boundary Layer Parameterizations, 25-27 November ECMWF. Also appears as MetO 20 Technical Note II/136, Meteorological Office, Bracknell.

Cheng, C-P., and Houze, R.A. 1979 — The distribution of convective and mesoscale precipitation in GATE radar echo patterns. Mon. Wea. Rev., 107, p426-441

Clarke, R.H. 1970 — Recommended methods for the treatment of the boundary layer in numerical models. Austr. Met. Mag., 18, p51-73

Gregory, D. 1986 — A numerical study of the parameterization of deep tropical convection. Ph.d Thesis, University of London.

Gregory, D., and Miller, M.J. 1988 — A numerical study of convective parameterization. (In preparation)

Lyne, W.H., and Rowntree, P.R. 1976 — Development of a convective parameterization using GATE data. MetO 20 Technical Note II/70, Meteorological Office, Bracknell.

Miller, M.J. and Pearce, R.P. 1974 — A three dimensional primitive equation model of cumulonimbus convection. Quart. J. R. Met. Soc., 110, p133-154

Rowntree, P.R. 1973 — Proposed convection scheme for the 11-layer tropical model. Unpublished typescript, MetO 20, Meteorological Office, Bracknell.

Slingo, A (ed) 1985 — Handbook of the Meteorological Office 11-layer atmospheric general circulation model. MetO 20 Technical Note 29, Meteorological Office, Bracknell.

Thompson, R.M., Payne, S.W., Recker, E.E., and Reed, R.J. 1979 — Structure and properties of synoptic scale wave disturbances in the intertropical convergence zone of the eastern Atlantic. J. Atmos. Sci., 36, p53-72

(9) NOTATION.

p_*	surface pressure
g	acceleration due to gravity
σ	p/p_*
$\Delta\sigma_k$	$\sigma_{k+1/2}-\sigma_{k-1/2}$
q	specific humidity
θ	potential temperature
ε	entrainment rate
η	mixing detrainment rate
δ	forced detrainment rate
M	convective massflux
φ_k	φ at layer k of model
$\varphi_{k-1/2}$	φ at upper layer boundary
$\varphi_{k+1/2}$	φ at lower layer boundary

Note that k decreases with σ, lowest model layer being layer 11, top model layer being layer 1.

Table 1 Vertically and horizontally integrated budgets of large-scale horizontal and vertical advective heating and moistening, surface fluxes and observed surface rainfall (interpolated to model 10 hour averaging periods from those in TPRR(1979)). Units are Wm^{-2}.

Time(hrs)	0-10	10-20	20-30	30-40	40-50	50-60	60-70	70-80
$-\pi\overline{\underline{v}.\nabla\theta} - \pi\bar{\omega}\frac{\partial\bar{\theta}}{\partial p}$	-303	-443	-542	-465	-277	-111	-58	-160
H	8	12	16	18	15	11	8	7
$L(-\overline{\underline{v}.\nabla q} - \bar{\omega}\frac{\partial\bar{q}}{\partial p})$	320	455	517	386	176	38	36	170
LE	86	100	114	122	123	122	113	92
Rain	107	379	541	619	616	281	214	143

$29 Wm^{-2} \equiv 1$mm/day

H ≡ sensible heat flux
LE≡ latent heat flux

Experiment number	Convection scheme	Changed constants
X1	3ac	evcon=3
X2	3ac	evcon=9
X3	4ac	$c=3.33\times10^{-4}$
X4	4ac	$c=3.33\times10^{-5}$

Table 2 Experiments performed in comparison of the 3rd and 4th annual cycle convection schemes.
(Note the 4th annual cycle scheme does not use evcon in the calculation of evaporation below cloud base.)

Experiment number	Net simulated rainfall over the wave (Wm^{-2})	Observed rainfall (Wm^{-2})	Net moisture forcing over the wave (Wm^{-2})
X1	367	363	371
X2	373	363	371
X3	358	363	371
X4	357	363	371

Table 3 Net rainfall averaged over the composite wave for experiments indicated - equilibrium with applied moisture forcing (large-scale plus surface fluxes).

Table 4 Mean temperature and moisture profiles for the first wave cycle ($\overline{\phi'}$) and composite wave cycle (2 to 6) ($\overline{\phi}$) compared to observations.

TEMPERATURE

Levels	Pressure (mb)	X2 (3ac,evcon=9)				X3 (4ac,c=3.33×10^{-4})			
		$\overline{T}$ (K)	T_{obs} (K)	$\overline{T'}-T_{obs}$ (K)	$\overline{T}-T_{obs}$ (K)	$\overline{T}$ (K)	T_{obs} (K)	$\overline{T'}-T_{obs}$ (K)	$\overline{T}-T_{obs}$ (K)
1	23	221.5	216.0	+1.4	+5.5	220.8	216.0	+1.1	+4.8
2	90	199.1	199.9	-0.4	-0.8	198.7	199.9	-0.6	-1.2
3	160	204.4	207.9	-1.0	-3.5	204.7	207.9	-1.0	-3.2
4	233	225.3	225.9	-0.6	-0.7	226.0	225.9	-0.2	+0.1
5	322	244.0	244.0	-0.1	0.0	244.3	244.0	-0.4	+0.3
6	442	260.9	260.4	+0.5	+0.5	261.6	260.4	+0.9	+1.2
7	585	273.1	272.6	+0.5	+0.5	272.7	272.6	+0.5	+0.1
8	727	282.5	282.9	-0.7	-0.4	283.2	282.9	+0.7	+0.3
9	855	289.1	289.7	-0.9	-0.6	289.8	289.7	+0.1	+0.1
10	950	293.7	294.2	-0.6	-0.5	295.1	294.2	+0.9	+0.9
11	1000	297.9	298.2	-0.3	-0.3	297.3	298.2	-0.9	-0.9

MOISTURE

Levels	Pressure (mb)	X2 (3ac,evcon=9)				X3 (4ac,c=3.33×10^{-4})			
		$\overline{q}$ (g/Kg)	q_{obs} (g/Kg)	$\overline{q'}-q_{obs}$ (g/Kg)	$\overline{q}-q_{obs}$ (g/Kg)	$\overline{q}$ (g/Kg)	q_{obs} (g/Kg)	$\overline{q'}-q_{obs}$ (g/Kg)	$\overline{q}-q_{obs}$ (g/Kg)
1	23	0.0	0.0	0.0	0.0	0.0	0.0	0.0	0.0
2	90	0.0	0.0	0.0	0.0	0.0	0.0	0.0	0.0
3	160	0.0	0.0	0.0	0.0	0.0	0.0	0.0	0.0
4	233	0.1	0.1	0.0	0.0	0.1	0.1	0.0	0.0
5	322	0.6	0.5	0.2	0.1	0.7	0.5	0.3	0.2
6	442	2.1	1.5	0.7	0.6	1.9	1.5	0.3	0.4
7	585	5.4	4.5	1.0	0.9	5.3	4.5	0.3	0.8
8	727	8.4	7.7	0.7	0.7	7.5	7.7	-0.5	-0.2
9	855	11.6	12.0	-0.6	-0.4	11.4	12.0	-0.7	-0.6
10	950	13.9	15.5	-2.0	-1.6	13.9	15.5	-1.5	-1.6
11	1000	15.6	17.2	-1.9	-1.6	17.9	17.2	0.8	0.7

Table5 Comparison of temperature and moisture composited over wave cycles 2 to 6 - deviations from observed wave averages.

Levels	Pressure (mb)	X1 (evcon=3)		X2 (evcon=9)	
		$\bar{T}-T_{obs}$ (K)	$\bar{q}-q_{obs}$ (g/Kg)	$\bar{T}-T_{obs}$ (K)	$\bar{q}-q_{obs}$ (g/Kg)
1	23	5.1	0.0	5.5	0.0
2	90	-0.9	0.0	-0.8	0.0
3	160	-3.2	0.0	-3.5	0.0
4	233	-0.4	0.0	-0.7	0.0
5	322	-0.3	0.2	0.0	0.1
6	442	0.6	0.4	0.5	0.6
7	585	0.3	0.6	0.5	0.9
8	727	-0.1	-0.2	-0.4	0.7
9	855	-0.4	-0.7	-0.6	-0.4
10	950	0.5	-1.9	-0.5	-1.6
11	1000	0.6	-1.6	-0.3	-1.6

Table6 Ratio of vertically integrated contributions of various terms to Q1 (averaged over wave cycles 2 to 6) - comparison of 3ac experiments and explicit model results for wave category three.

	Explicit model	3ac evcon=3	3ac evcon=9
$(Q1)_{conv}$	$527 Wm^{-2}$	$613 Wm^{-2}$	$635 Wm^{-2}$
UD/Q1	2.36	1.51	2.47
DD/Q1 (+) DEVP/Q1	-0.99 (=-1.36) -0.37	-0.45	-1.38

$(Q1)_{conv}$ ≡contribution of convection to Q1

For the explicit model
UD ≡contribution of updraught to Q1
DD ≡contribution of downdraught to Q1
DEVP ≡contribution of detrainment of liquid water to Q1

For 3ac version of Rowntree scheme
UD ≡contribution of subsidence, plus forced detrainment
DD+DEVP ≡contribution of evaporation

Table7 Ratio of vertically integrated contributions of various terms to Q1 (averaged over wave cycles 2 to 6) - comparison of 4ac experiments (X3) and explicit model results for wave category three.

	Explicit model	4ac $c=3.33\times10^{-4}$
$(Q1)_{conv}$	$527 Wm^{-2}$	$541 Wm^{-2}$
UD/Q1	2.39	1.26
DD/Q1	-0.99	-0.08
(+)	(=-1.36)	(=-0.23)
DEVP/Q1	-0.37	-0.15

$(Q1)_{conv}$ ≡contribution of convection to Q1

For the explicit model
UD ≡contribution of updraught to Q1
DD ≡contribution of downdraught to Q1
DEVP ≡contribution of detrainment of liquid water to Q1

For 4ac version of Rowntree scheme
UD ≡contribution of subsidence, plus forced and mixing detrainment
DD ≡contribution of evaporation below cloud base
DEVP ≡detrainment of liquid cloud water

(NOTE : 4ac definition of UD, DD and DEVP are different from 3ac definitions.)

Table 8 Contribution of large-scale and convective rainfall to total rainfall for the 3ac and 4ac schemes (averaged over wave cycles 2 to 6).

Scheme	Large-scale rain (Wm^{-2})	Convective rain (Wm^{-2})	Total rain (Wm^{-2})
3ac (X2)	1	311	312
4ac (X3)	12	298	310

Table 9 Mean temperature and moisture profiles for the first wave cycle ($\bar{\phi}^1$) and composite wave cycle (2 to 6) ($\bar{\phi}$) compared to observations for the modified 4ac scheme (improved downdraught representation).

Levels	Pressure (mb)	Temperature				Moisture			
		$\bar{T}$ (K)	T_{obs} (K)	$\bar{T}^1-T_{obs}$ (K)	$\bar{T}-T_{obs}$ (K)	q (g/Kg)	q_{obs} (g/Kg)	q^1-q_{obs} (g/Kg)	$\bar{q}-q_{obs}$ (g/Kg)
1	23	221.3	216.0	+1.3	+5.3	0.0	0.0	0.0	0.0
2	90	198.8	199.9	-0.6	-1.1	0.0	0.0	0.0	0.0
3	160	204.8	207.9	-1.0	-3.1	0.0	0.0	0.0	0.0
4	233	226.2	225.9	-0.7	+0.3	0.1	0.1	0.0	0.0
5	322	244.9	244.0	-0.4	+0.9	0.7	0.5	0.3	0.2
6	442	261.7	260.4	+0.5	+1.3	2.3	1.5	0.7	0.8
7	585	272.9	272.6	+0.1	+0.3	5.8	4.5	-1.4	1.3
8	727	282.9	282.9	-0.7	0.0	8.6	7.7	-1.0	0.9
9	855	289.3	289.7	-1.1	-0.4	12.0	12.0	-0.4	0.0
10	950	293.8	294.2	-0.8	-0.4	14.5	15.5	-1.4	-1.0
11	1000	296.7	298.2	-1.9	-1.5	17.0	17.2	-0.6	-0.2

Table10 Comparison of saturation level of free convection for several experiments compared to observations (composite profiles over wave cycles 2 to 6).

Experiment	Saturation level (from 1000mb)	Level of free convection (from 1000mb)
X2(3ac)	940mb	≃860mb
X3(4ac)	960mb	≃950mb
Modified 4ac(evcon=9)	970mb	≃930mb
Observed	959mb	≃935mb

Table11 Ratio of vertically integrated contributions of various terms to Q1 (averaged over wave cycles 2 to 6) - comparison of modified 4ac experiments and explicit model results for wave category three.

	Explicit model	Modified 4ac
$(Q1)_{conv}$	$527 Wm^{-2}$	$500 Wm^{-2}$
UD/Q1	2.39	2.34
DD/Q1	-0.99	-1.04
(+)	(=-1.36)	(=-1.28)
DEVP/Q1	-0.37	-0.24

$(Q1)_{conv}$ ≡contribution of convection to Q1

For the explicit model
- UD ≡contribution of updraught to Q1
- DD ≡contribution of downdraught to Q1
- DEVP ≡contribution of detrainment of liquid water to Q1

For modified 4ac version of Rowntree scheme
- UD ≡contribution of subsidence, plus forced and mixing detrainment
- DD ≡contribution of evaporation of precipitation
- DEVP ≡detrainment of liquid cloud water

Table12 Comparison of standard and modified en/detrainment rates used in the Rowntree convection scheme experiments.

STANDARD	MODIFIED
ENTRAINMENT For all levels $\epsilon_{k-1/4}=3A_E\sigma_k(\sigma_k-\sigma_{k-1/2})$ $\epsilon_{k-3/4}=3A_E\sigma_{k-1/2}(\sigma_{k-1/2}-\sigma_{k-1})$	ENTRAINMENT For all levels $\epsilon_{k-1/4}=3A_E\sigma_k(\sigma_k-\sigma_{k-1/2})$ $\epsilon_{k-3/4}=3A_E\sigma_{k-1/2}(\sigma_{k-1/2}-\sigma_{k-1})$
MIXING DETRAINMENT $\eta_k=(\epsilon_{k-1/4}+\epsilon_{k-3/4})(1-1/A_E)$ $A_E=1 \quad k=11$ $A_E=1.5 \quad k<11$	MIXING DETRAINMENT For layers 11,10,9 $\eta_k=(\epsilon_{k-1/4}+\epsilon_{k-3/4})/4$ For layers 8 to 1 $(1-\eta_k)=\left\{\frac{\beta}{(1+\epsilon_{k-1/4})(1+\epsilon_{k-3/4})}+(1-\beta)\right.$ $A_E=1 \quad k=11$ $A_E=1.5 \quad k<11$

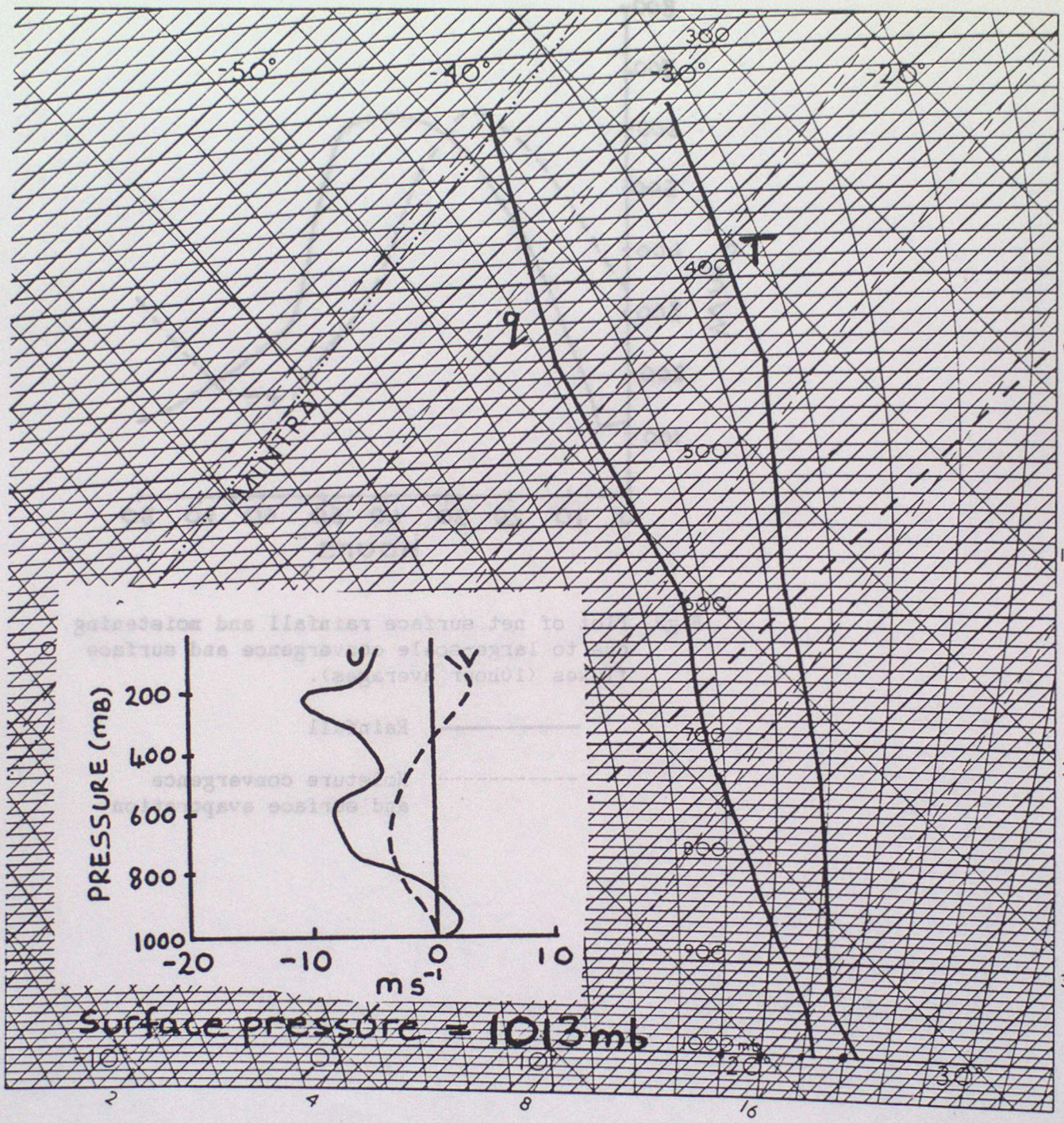

Fig1 T, q, u and v profiles for 2.5hours of the TPRR data set (0 hours model time).

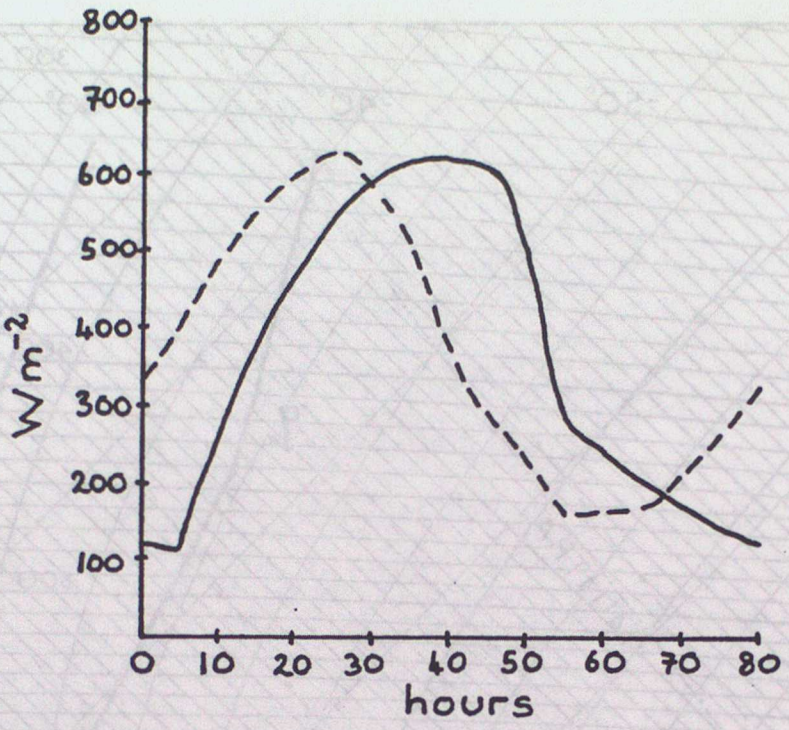

Fig2 Plot of net surface rainfall and moistening due to large-scale convergence and surface fluxes (10hour averages).

——————— Rainfall

---------- Moisture convergence and surface evaporation

Fig3 Observed Q1 and Q2 with forcing applied to the model

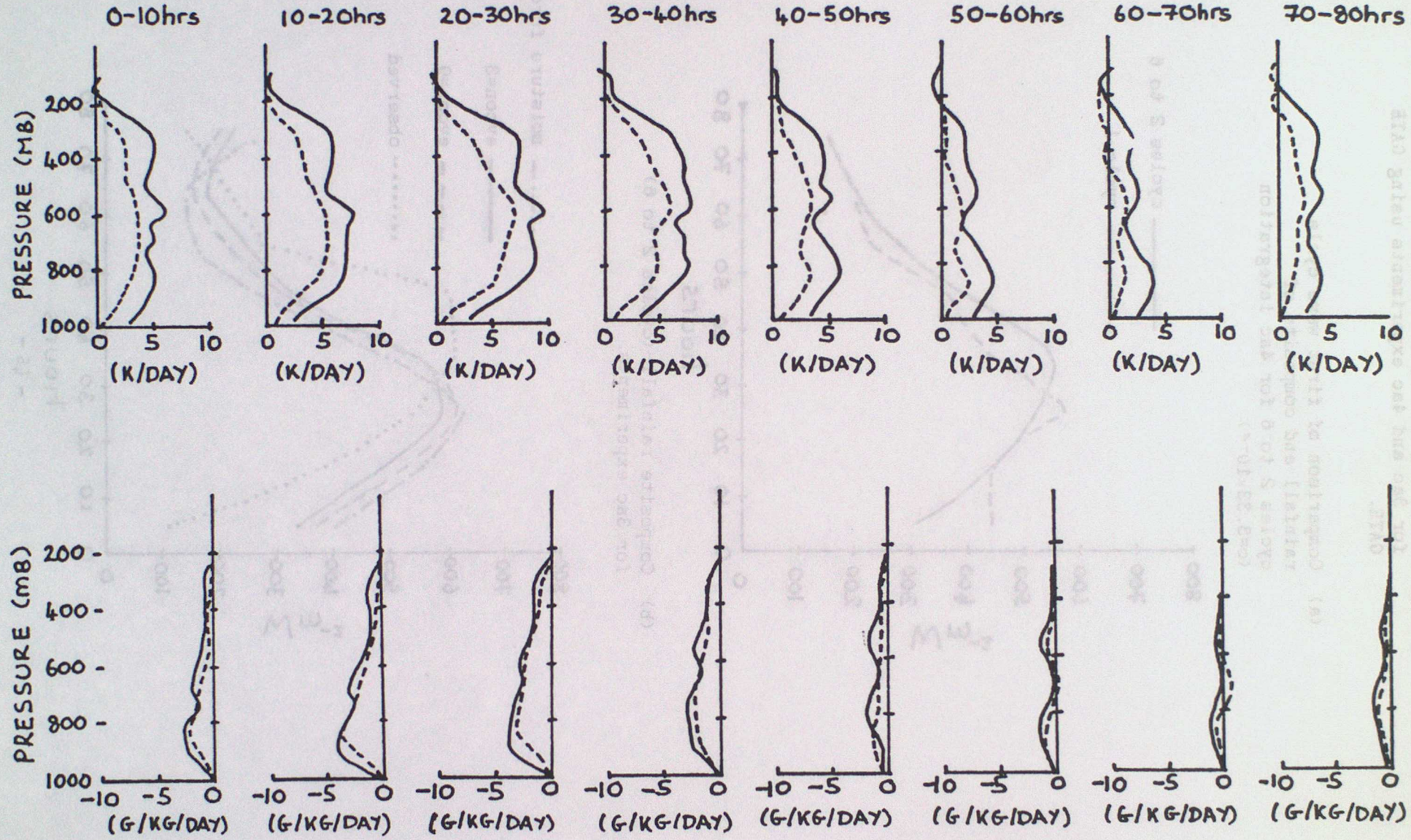

Fig4 10 hourly average convective rainfall for 3ac and 4ac experiments using GATE GATE.

(a) Comparison of first wave cycle rainfall and composite of cycles 2 to 6 for 4ac integration ($c=3.33\times10^{-4}$)

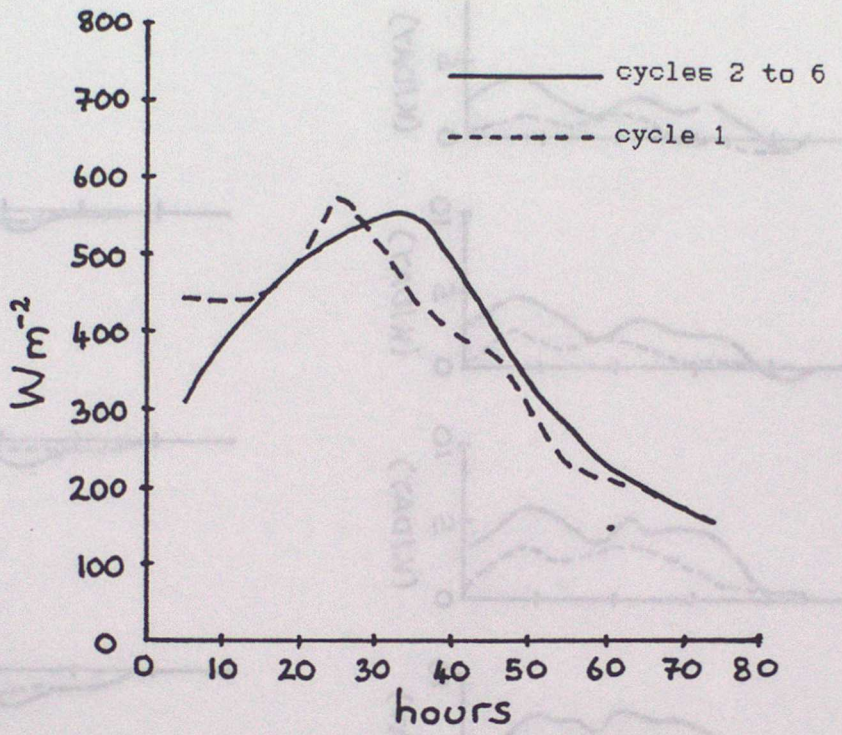

(b) Composite rainfall (cycles 2 to 6) for 3ac experiments.

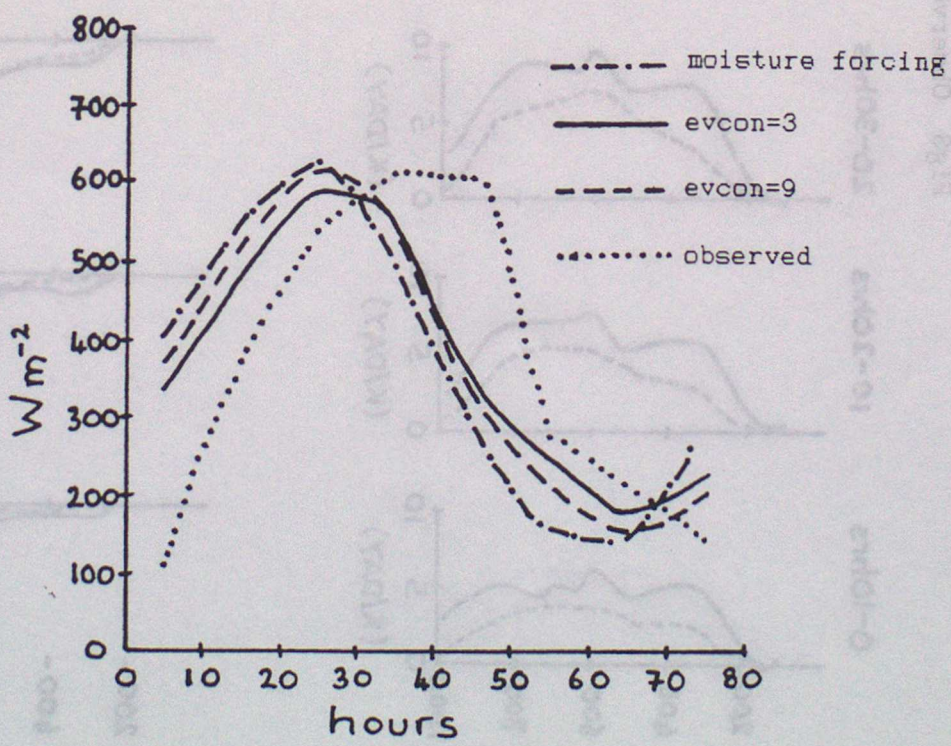

Fig 4 cont.

(c) Composite rainfall (cycles 2 to 6) for 4ac experiments.

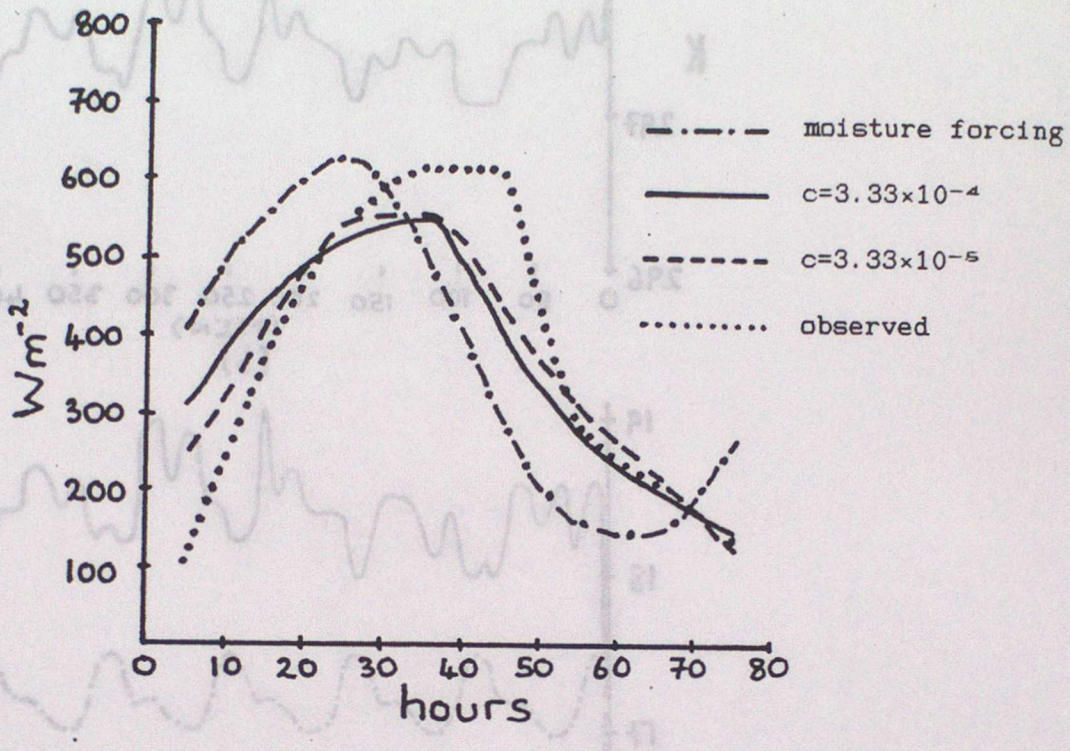

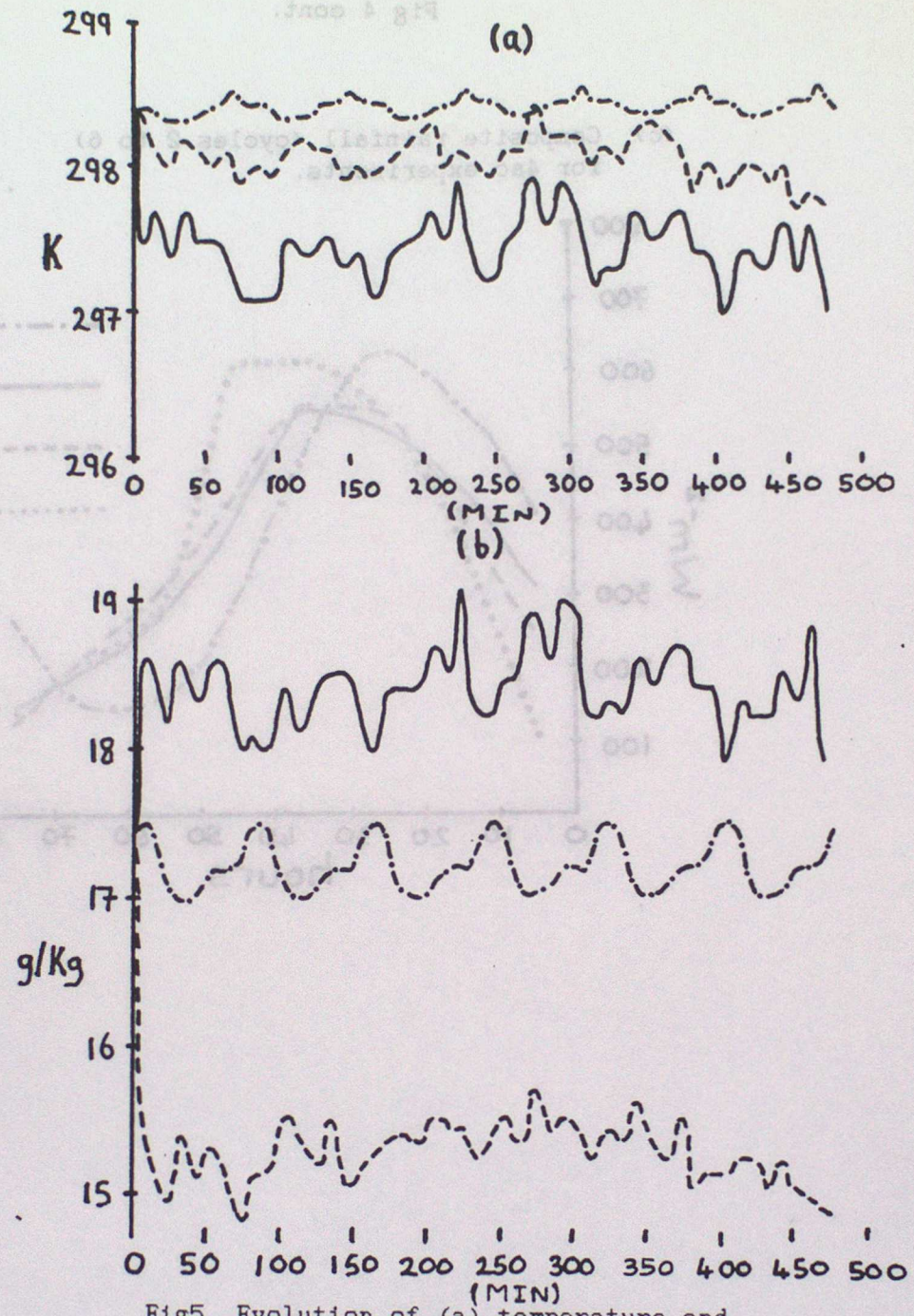

Fig5 Evolution of (a) temperature and (b) mixing ratio of the lowest model layer for experiments X2 and X3 (see table2)

X3 ———— (4ac, c=3.33×10⁻⁴)

X2 ---------- (3ac, evcon=9)

observed -·-·-·-·-

Initial values

T_{1000mb}=298.4K

q_{1000mb}=17.4g/Kg

(Experiments X1 and X4 give similar results to X2 and X3 respectively)

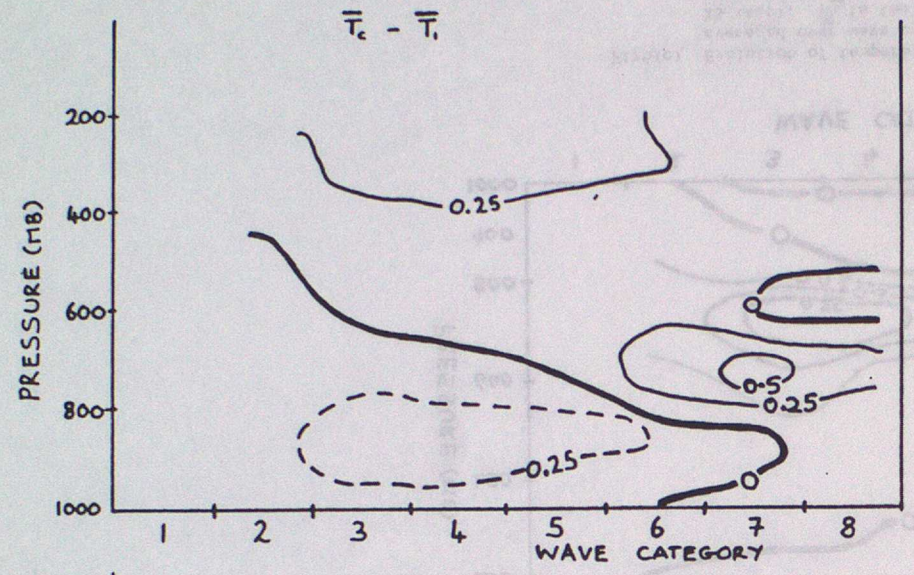

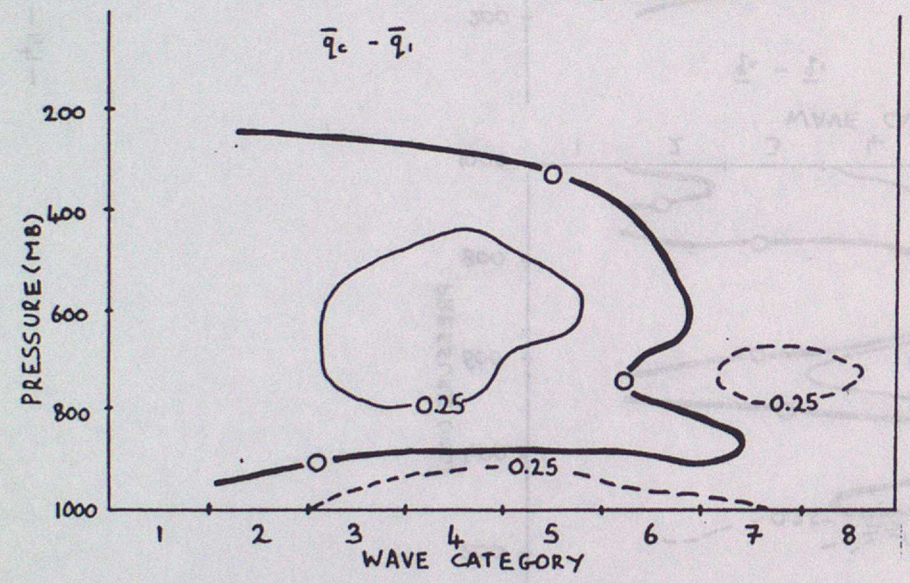

Fig6(a) Evolution of temperature and moisture profiles for a composite easterly wave (TPRR(1979)). Observed values. $\overline{\phi}_c$ is the mean of ϕ for wave category c, $\overline{\phi}_1$ is the mean for wave category 1.

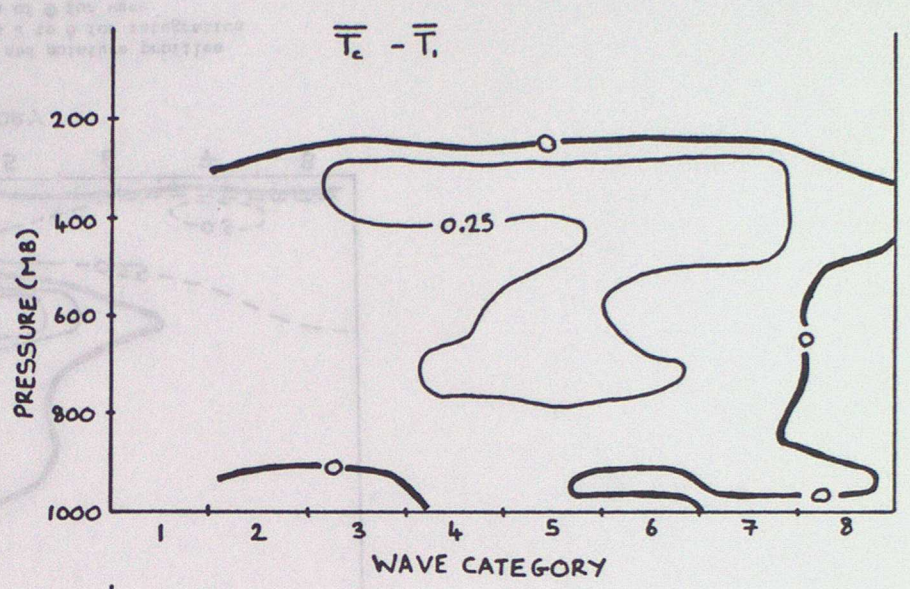

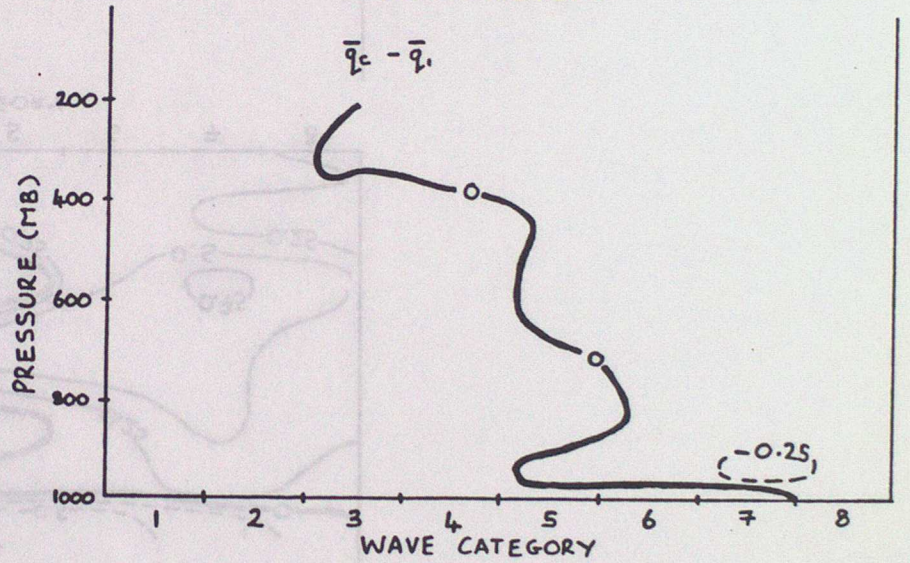

Fig6(b) Evolution of temperature and moisture profiles averaged over wave cycles 2 to 6 for integration X2 (3ac). $\overline{\phi}_c$ is the mean for wave category c, $\overline{\phi}_1$ is the mean of ϕ for wave category 1.

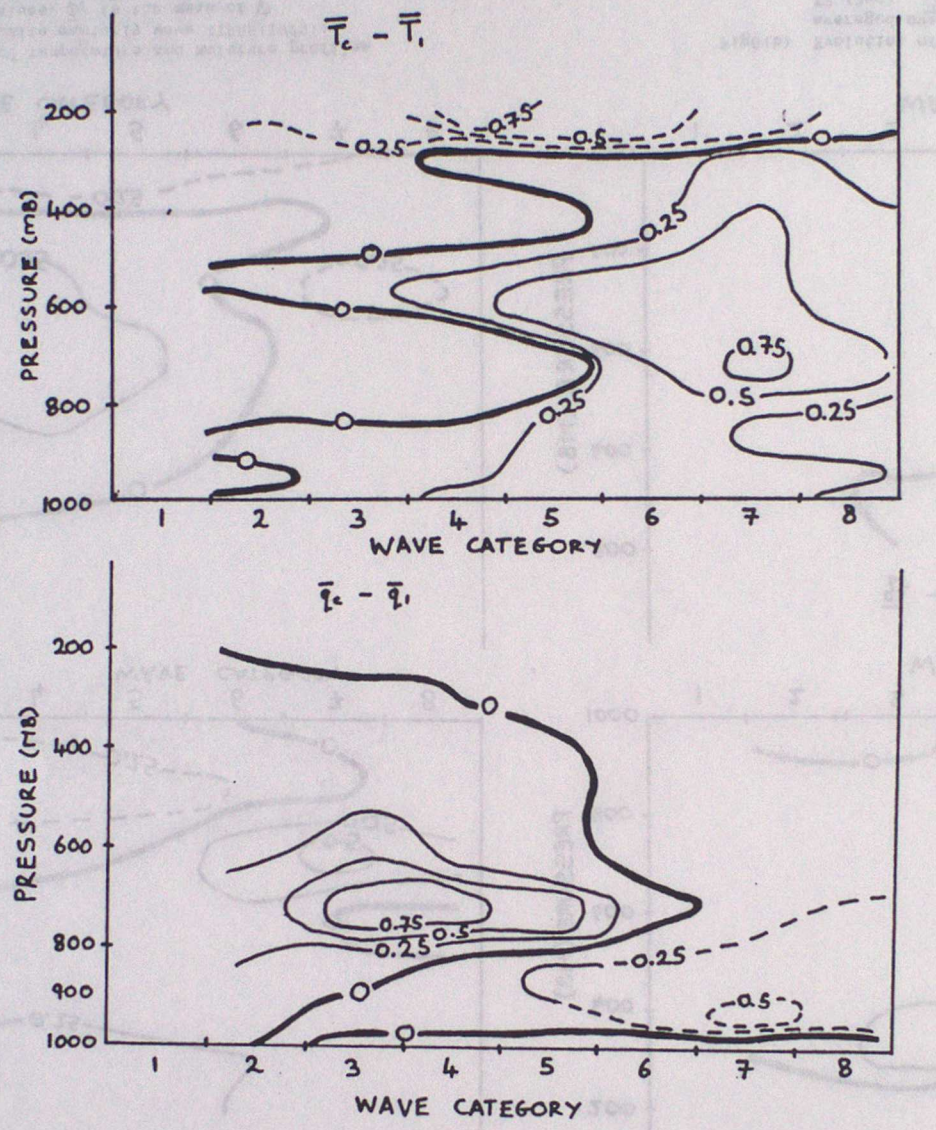

Fig6(c) Evolution of temperature and moisture profiles averaged over wave cycles 2 to 6 for integration X3 (4ac). $\overline{\phi}_c$ is the mean of ϕ for wave category c, $\overline{\phi}_1$ is the mean of ϕ for wave category 1.

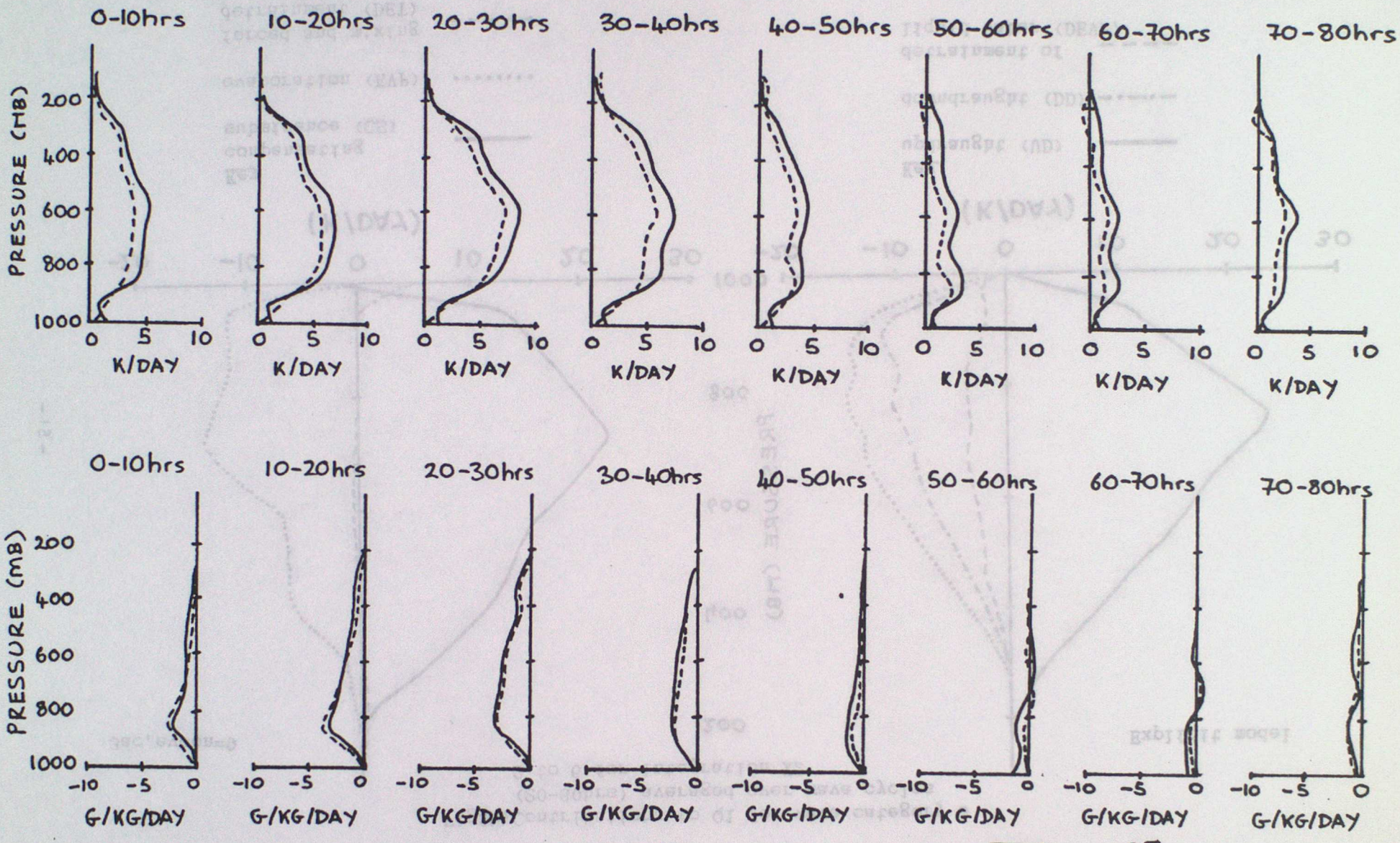

Fig7 Evolution of Q1 and Q2 through a wave cycle (averaged over wave cycles 2 to 6) for integration X2

Fig8(a) Contributions to Q1 for wave category 3 (20-30hrs) averaged over wave cycles 2 to 6 for integration X2

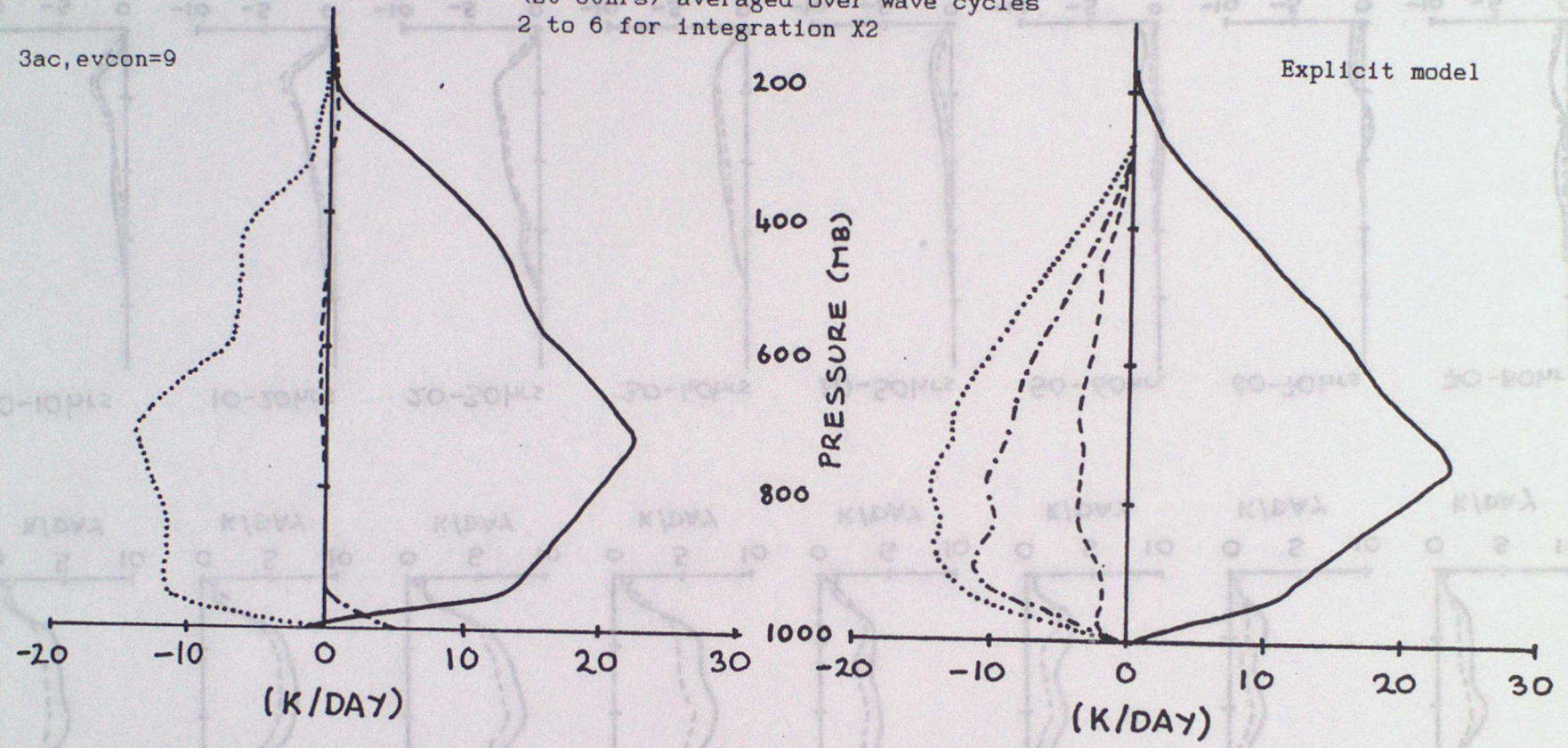

Key
compensating subsidence (CS)
evaporation (EVP)
forced and mixing detrainment (DET)
boundary layer (BL)

Key
updraught (UD)
downdraught (DD)
detrainment of liquid water (DEVP)
(DD+DEVP)

Fig 8 cont. Contributions to Q2.

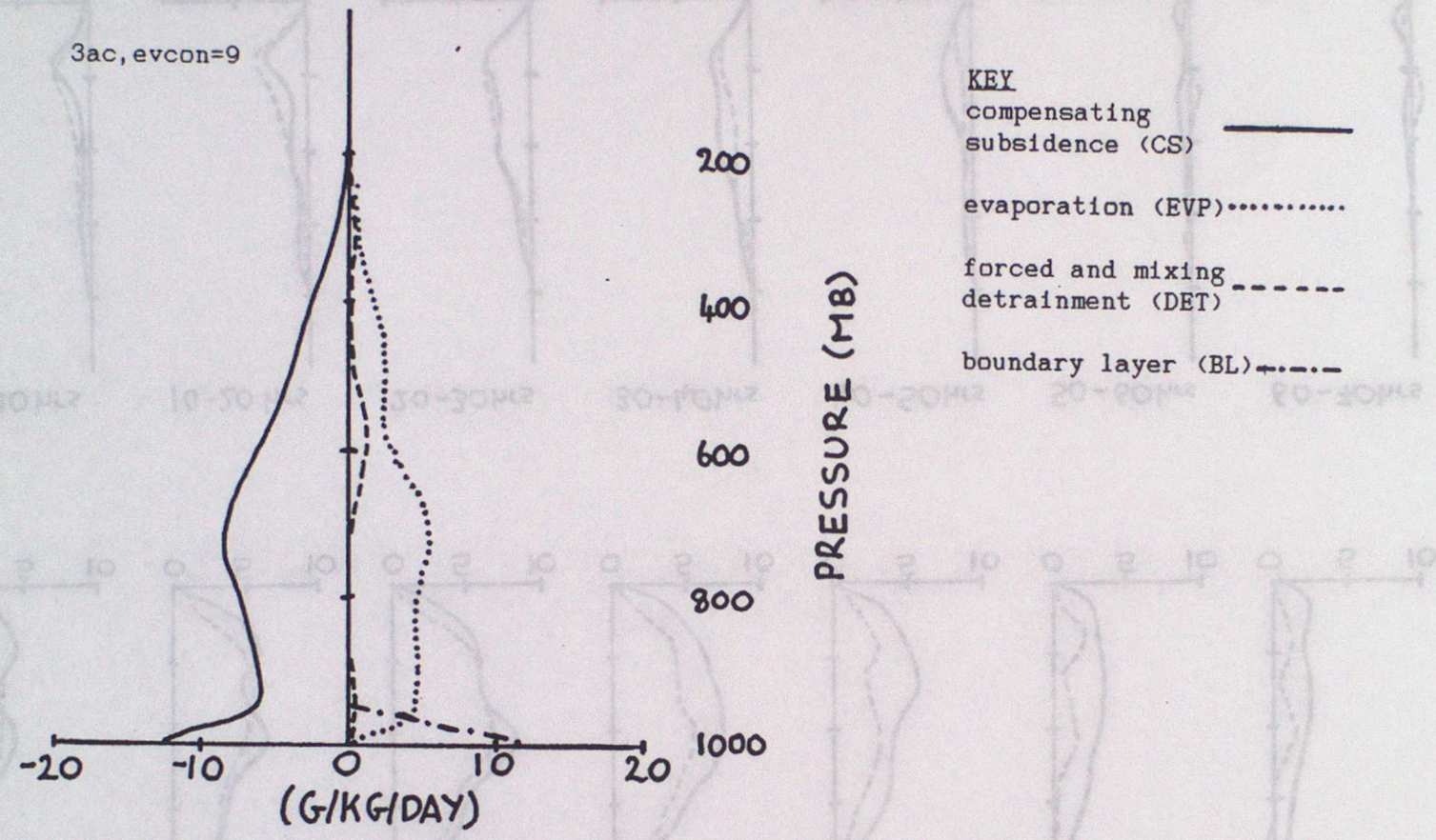

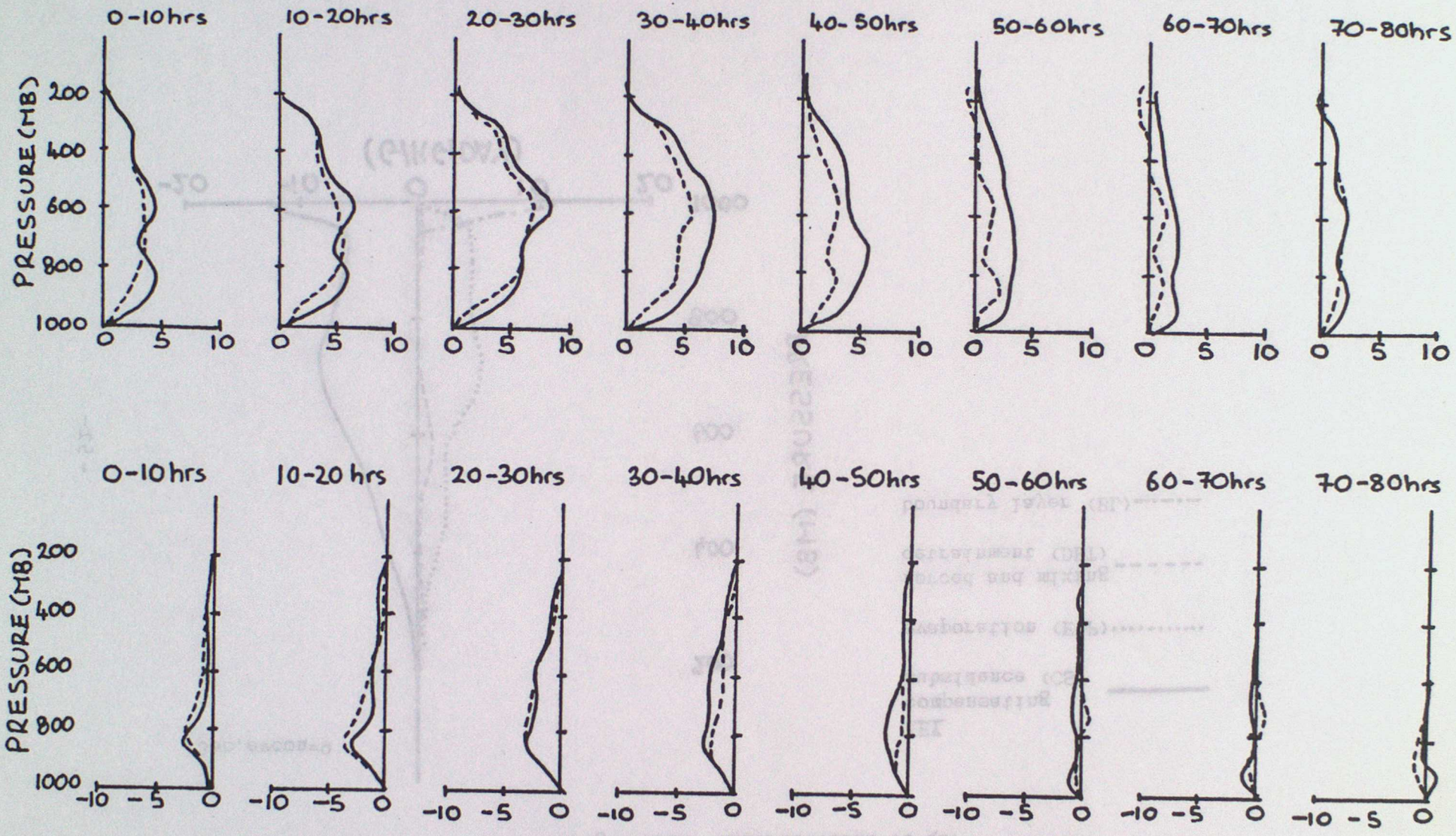

Fig 9 Evolution of Q1 and Q2 through a wave cycle (averaged over wave cycles 2 to 6) for integration X3.

Fig 10 Contributions to Q1 and Q2 for wave category 3 (20-30hours) averaged over wave cycles 2 to 6 for integrations X3.

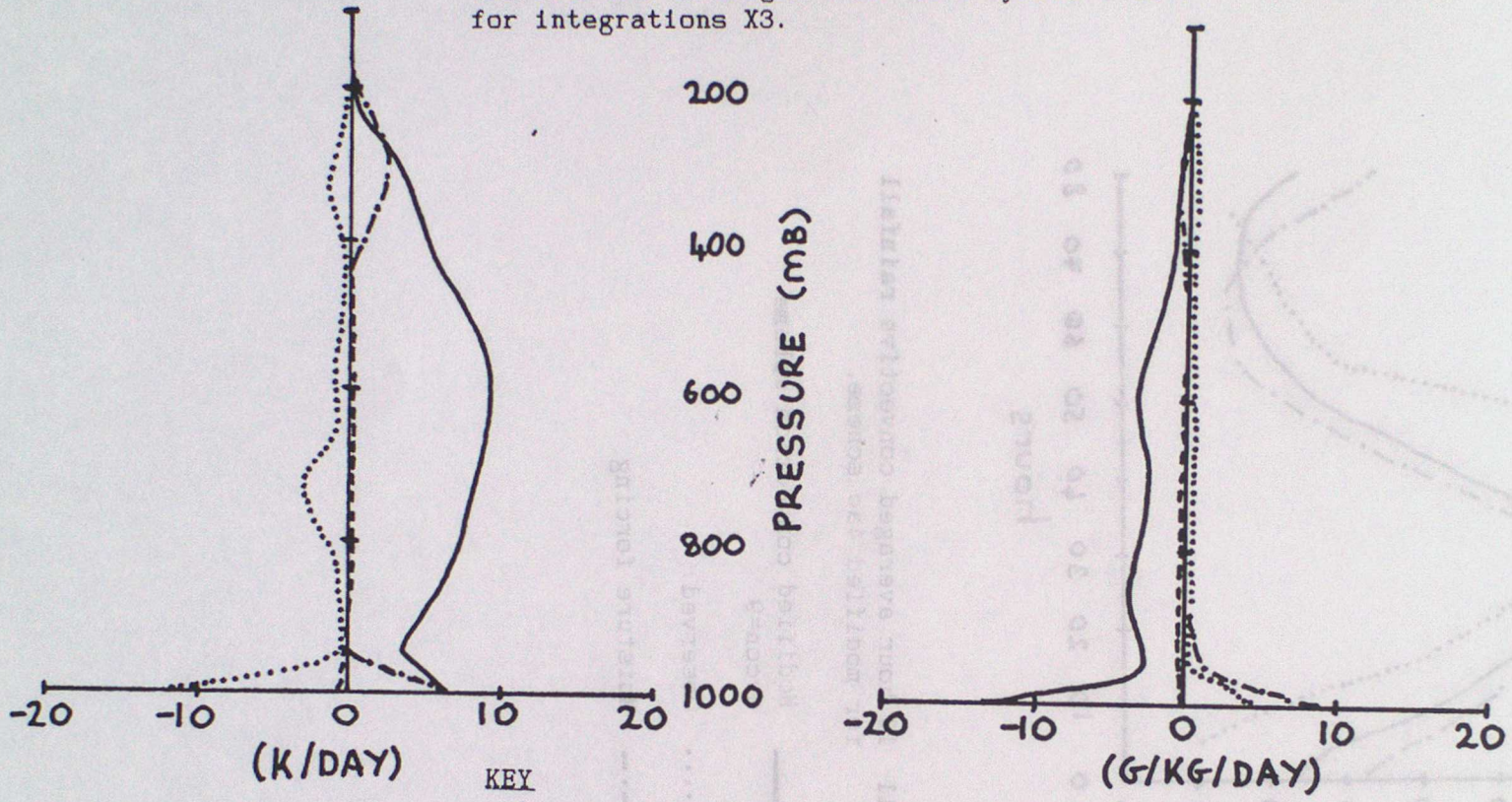

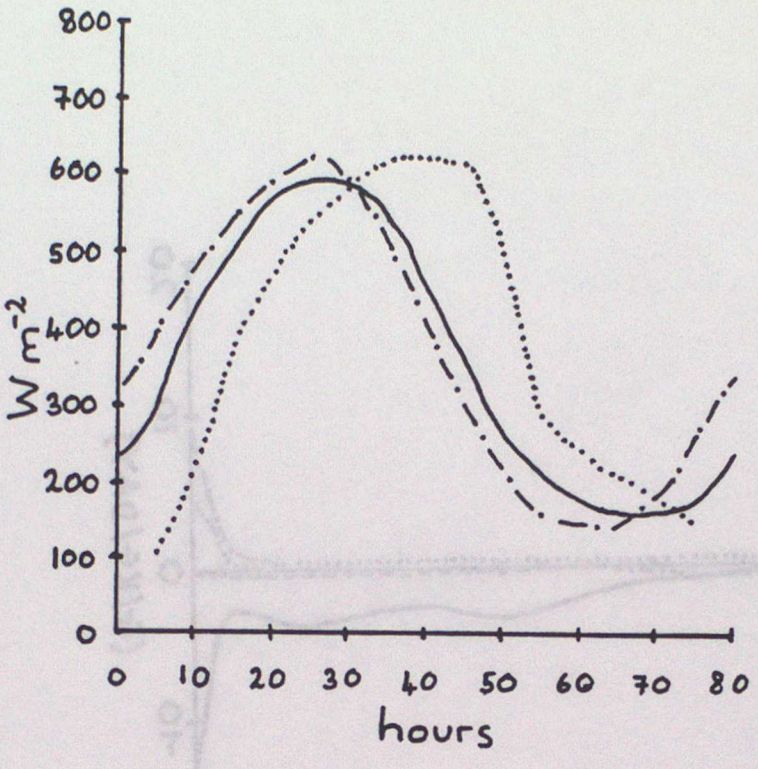

Fig 11 10 hour averaged convective rainfall for modified 4ac scheme.

——— Modified convection scheme evcon=9

..... Observed

—·—·— Moisture forcing

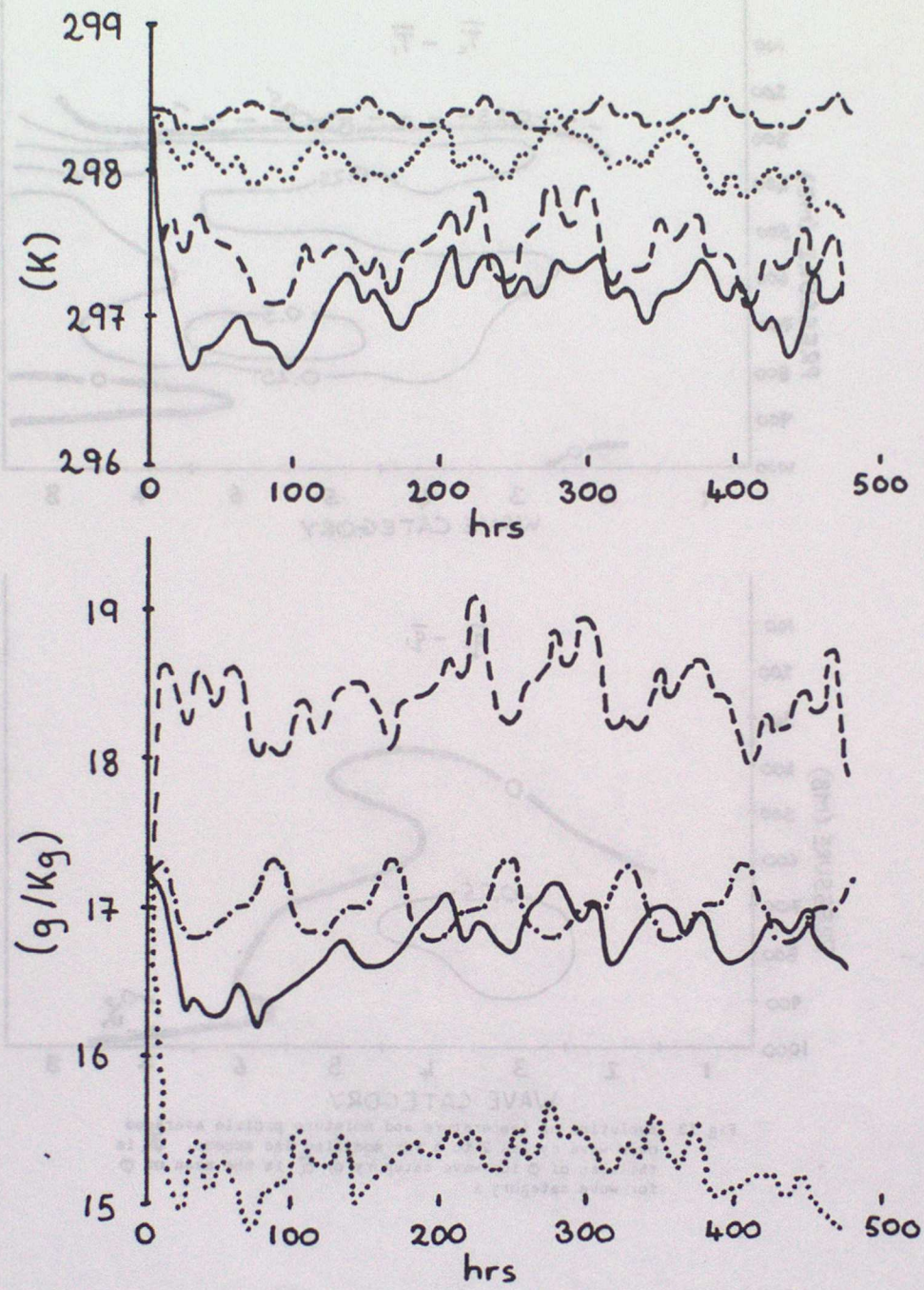

Fig 12 Comparison of the evolution of T_{11} and q_{11} for 3ac (evcon=9), 4ac and modified 4ac (evcon=9) convection schemes.

Averaged T_{11} and q_{11} for cycles 2 to 6.

	T_{11} (K)	q_{11} (g/Kg)
3ac	298.0	15.7
4ac	297.5	18.4
mod.4ac	297.1	16.8
observed	298.4	17.2

——— Modified 4ac (evcon=9)

- - - - 4ac

····· 3ac (evcon=9)

—·—·— Observed

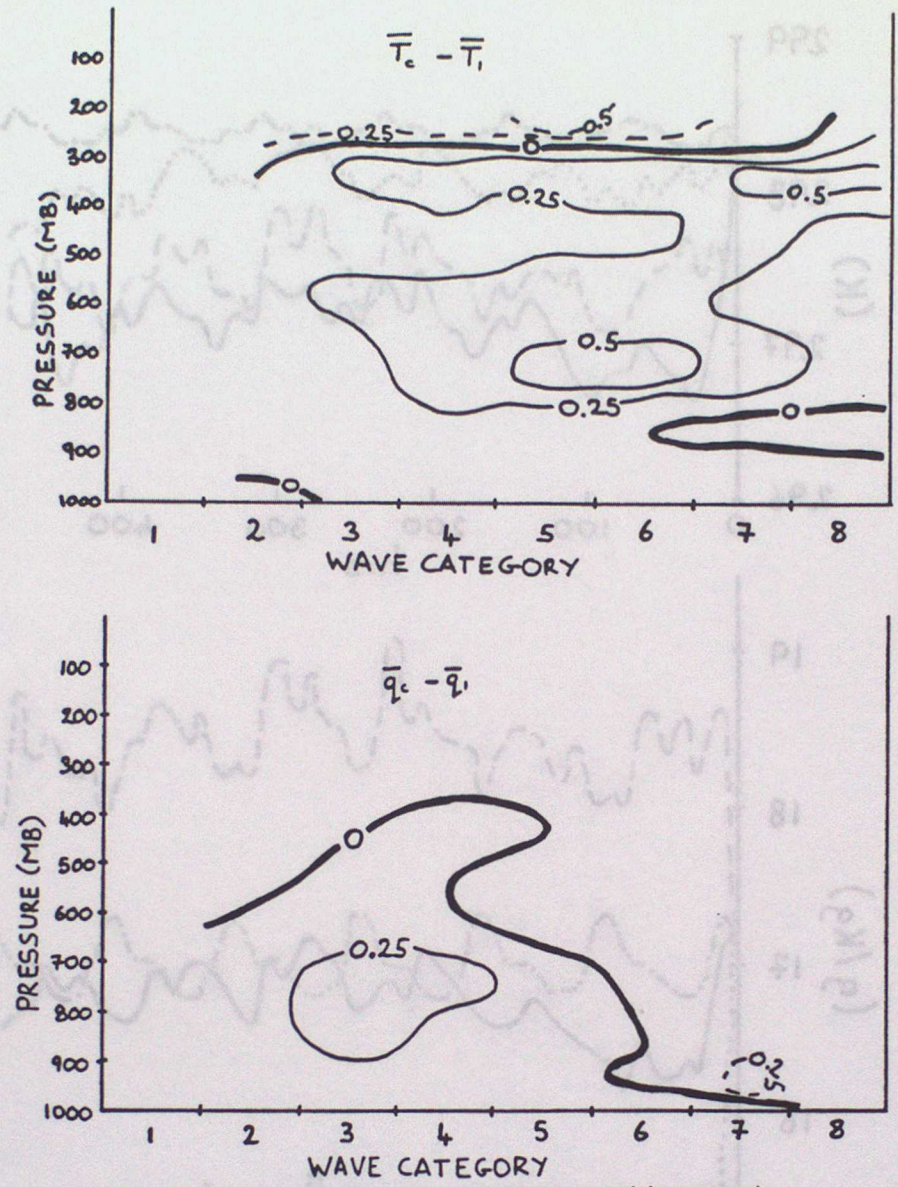

Fig 13 Evolution of temperature and moisture profile averaged over wave cycles 2 to 6 for modified 4ac scheme. $\overline{\phi}_c$ is the mean of ϕ for wave category c, $\overline{\phi}_1$ is the mean of ϕ for wave category 1.

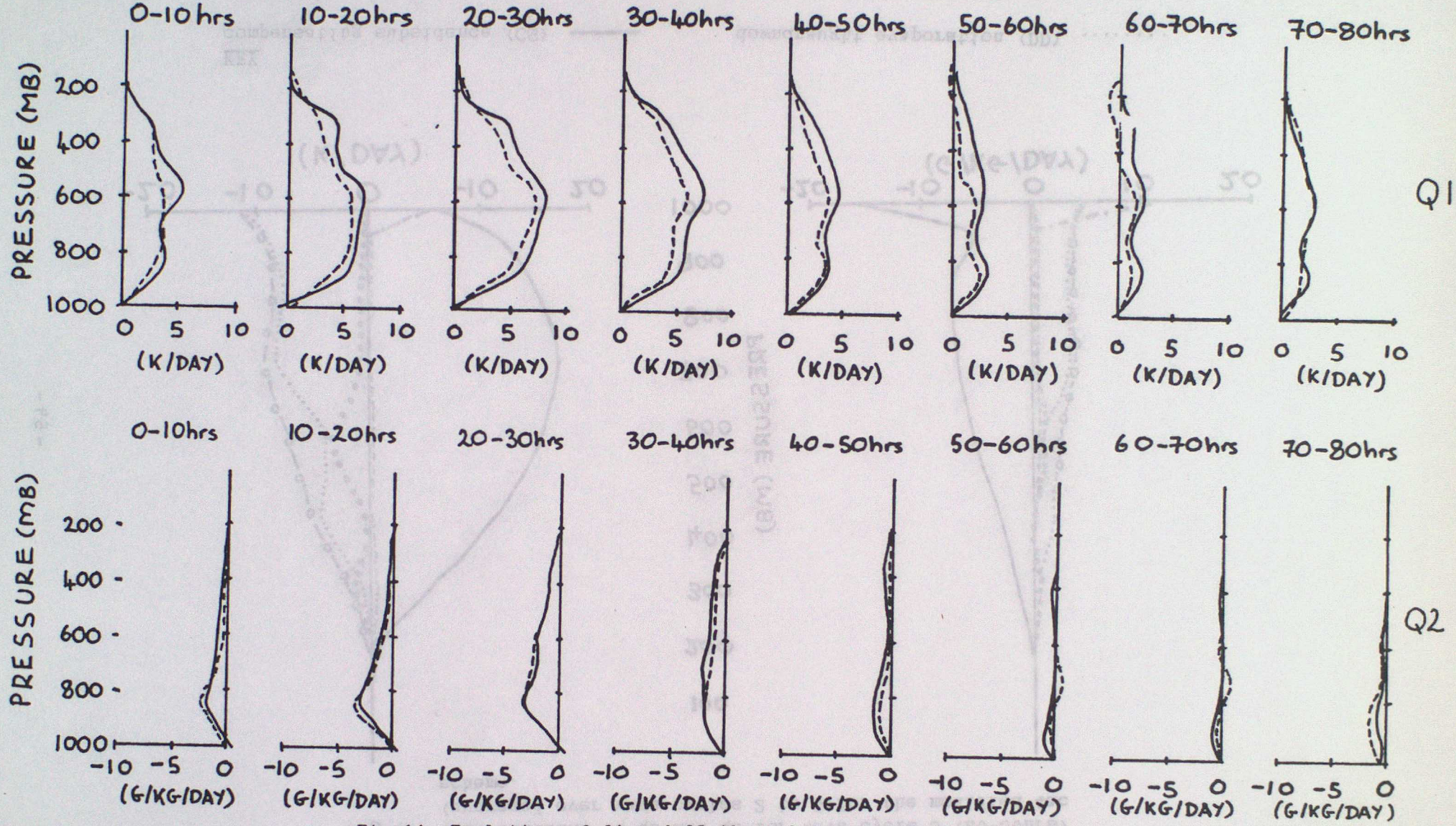

Fig 14 Evolution of Q1 and Q2 through a wave cycle (averaged over wave cycles 2 to 6) for the modified 4ac scheme.

Q1 ——— $\pi \underline{v} \cdot \overline{\nabla\theta} + \pi\bar{\omega}\frac{\partial\bar{\theta}}{\partial p}$

Q2 - - - - - $\overline{\underline{v} \cdot \nabla q} + \bar{\omega}\frac{\partial\bar{q}}{\partial p}$

Fig 15 Contributions to Q1 and Q2 for wave cycle 3 (20-30hrs) (averaged over wave cycles 2 to 6)for the modified 4ac scheme.

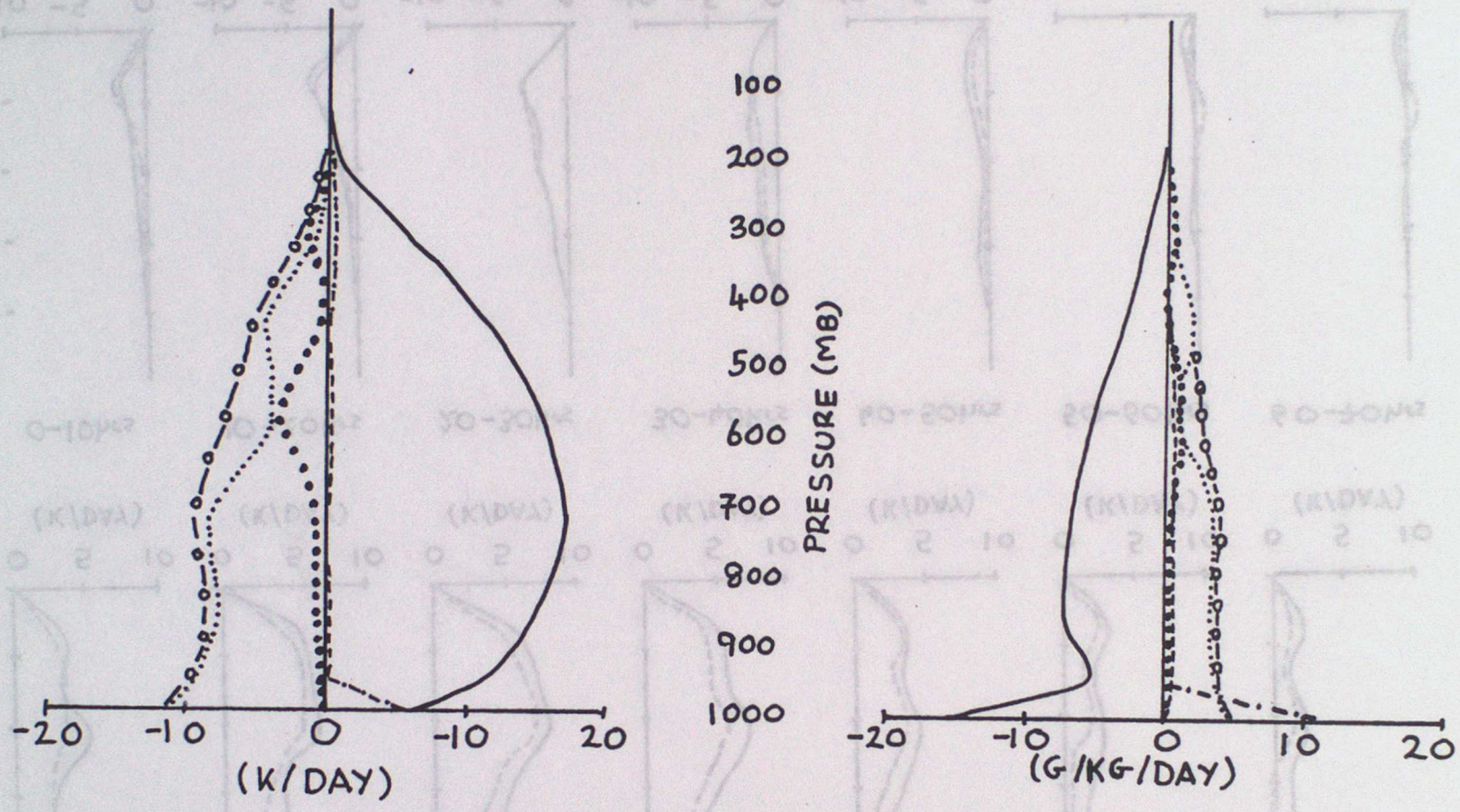

KEY

compensating subsidence (CS) ——

forced plus mixing detrainment (DET) - - - - -

evaporation of detrained cloud water (DEVP) ••••••

downdraught evaporation (DD) .....

boundary layer (BL) and large-scale rain (LSR) -.-.-.-

(DD+DEVP) o-o-o-

Fig 16 Comparison of the initial evolution of the standard 4th annual cycle and the 4th annual cycle with a downdraught representation. Deviation of temperature from the initial profile (K). Mixing ratio in g/kg.

4th annual cycle

Layer	T_{init}	hours 10	20	30	40
1	216.0				
2	199.7				
3	207.9				
4	225.9				
5	243.8				
6	260.4				
7	272.4				
8	282.9				
9	290.0				
10	294.5				
11	298.4				
q_{11}	17.4	18.6	18.6	18.2	18.6
$\Delta T \Delta\sigma$ ($\times 10^{-3}$)		85	127	-42	376

4th annual cycle plus downdraught (evcon=9)

Layer	T_{init}	hours 10	20	30	40
1	216.0				
2	199.7				
3	207.9				
4	225.9				
5	243.8				
6	260.4				
7	272.4				
8	282.9				
9	290.0				
10	294.5				
11	298.4				
q_{11}	17.4	16.9	16.4	16.2	16.5
$\Delta T \Delta\sigma$ ($\times 10^{-3}$)		-446	-471	-582	-198

observations

Layer	T_{init}	hours 10	20	30	40
1	216.0				
2	199.7				
3	207.9				
4	225.9				
5	243.8				
6	260.4				
7	272.4				
8	282.9				
9	290.0				
10	294.5				
11	298.4				
q_{11}	17.4	17.5	17.2	17.0	17.0
$\Delta T \Delta\sigma$ ($\times 10^{-3}$)		-72	-41	-18	14

Fig 17 Initial evolution of temperature for several integrations with modified en/detrainment rates.
Deviation of temperature from the initial profile (K). Mixing ratio in g/kg.

(a) β=3, layer 8 to 1
evcon=9
$c=2.22\times10^{-4}$

Layer	T_{init}	hours 10	20	30	40
1	216.0				
2	199.7				
3	207.9				
4	225.9				
5	243.8				
6	260.4				
7	272.4				
8	282.9				
9	290.0				
10	294.5				
11	298.4				
q_{11}	17.4	17.2	16.8	16.5	16.7
$\Delta T\Delta\sigma$ ($\times10^{-3}$)		-397	-447	-622	-255

(b) β=2, layer 8
β=4, layers 7 to 1
evcon=9
$c=1.62\times10^{-4}$

Layer	T_{init}	hours 10	20	30	40
1	216.0				
2	199.7				
3	207.9				
4	225.9				
5	243.8				
6	260.4				
7	272.4				
8	282.9				
9	290.0				
10	294.5				
11	298.4				
q_{11}	17.4	17.3	16.8	16.4	17.0
$\Delta T\Delta\sigma$ ($\times10^{-3}$)		-446	-471	-582	-198

(c) β=2 layer 8
β=4, layers 7 to 1
evcon=9, layers 11, 10
evcon=6, layers 9, 8
evcon=4, layers 7 to 1
$c=1.62\times10^{-4}$

Layer	T_{init}	hours 10	20	30	40
1	216.0				
2	199.7				
3	207.9				
4	225.9				
5	243.8				
6	260.4				
7	272.4				
8	282.9				
9	290.0				
10	294.5				
11	298.4				
q_{11}	17.4	17.4	17.0	16.6	16.8
$\Delta T\Delta\sigma$ ($\times10^{-3}$)		-97	-150	-396	-64